NASA TECHNICAL MEMORANDUM

NASA TM X-73,158 C./

NASA TM X-73,158

PREDICTED DYNAMIC CHARACTERISTICS OF THE XV-15 TILTING PROPROTOR AIRCRAFT IN FLIGHT AND IN THE 40- BY 80-FT WIND TUNNEL

Wayne Johnson

Ames Research Center
and
Ames Directorate
U.S. Army Air Mobility R&D Laboratory
Moffett Field, California 94035

June 1976

1. Report No.	2. Government Accession No.	3. Recipient's Catalog No.
NASA TM X-73,158		

4. Title and Subtitle	5. Report Date
PREDICTED DYNAMIC CHARACTERISTICS OF THE XV-15 TILTING PROPROTOR AIRCRAFT IN FLIGHT AND IN THE 40- BY 80-FT WIND TUNNEL	6. Performing Organization Code

7. Author(s)	8. Performing Organization Report No.
Wayne Johnson	A-6700
	10. Work Unit No. 505-10-22

9. Performing Organization Name and Address	11. Contract or Grant No.
NASA Ames Research Center and Ames Directorate, U.S. Air Mobility R&D Laboratory Moffett Field, California 94035	

12. Sponsoring Agency Name and Address	13. Type of Report and Period Covered
NASA, Washington, D.C. 20546 and U.S. Army Air Mobility R&D Laboratory, Moffett Field, California 94035	Technical Memorandum
	14. Sponsoring Agency Code

15. Supplementary Notes

16. Abstract

Pretest predictions of the dynamic characteristics of the XV-15 tilting proprotor aircraft are presented. The data for the aircraft in flight includes: trim conditions, flight dynamics, gust response, aeroelastic stability, and wing response to control. The data for the aircraft in the Ames 40- by 80-Ft Wind Tunnel includes aeroelastic stability, and the wing response to control. The calculations were made for pylon tilt angles of 0° (airplane mode), 0.1° (pylon unlocked), 30°, 60°, and 90° (helicopter mode).

17. Key Words (Suggested by Author(s))	18. Distribution Statement
Tiltrotor aircraft Flight dynamics Aeroelastic stability	Unlimited STAR Category - 01

19. Security Classif. (of this report)	20. Security Classif. (of this page)	21. No. of Pages	22. Price*
Unclassified	Unclassified	56	$4.25

*For sale by the National Technical Information Service, Springfield, Virginia 22161

NOMENCLATURE

a_x	longitudinal acceleration
a_y	lateral acceleration
a_z	vertical acceleration
h	altitude of aircraft CG above ground level
p	wing torsion mode
q_1	wing vertical bending mode
q_2	wing chordwise bending mode
$t_{\frac{1}{2}}$	time to half amplitude
T	Period
α	pylon yaw mode
α_p	pylon tilt angle; 0. for airplane mode, 90° for helicopter mode; $\alpha_p = 0.1^\circ$ is airplane mode with pylon unlocked
δ_s	cyclic stick position
ζ	damping ratio of root
θ_f	aircraft trim pitch angle
$\theta_{.75}$	rotor collective pitch angle at 75% radius
λ	eigenvalue or root of system; dimensionless, based on rotor rotational speed.
σ_G	rms gust velocity

PREDICTED DYNAMIC CHARACTERISTICS OF THE XV-15 TILTING PROPROTOR AIRCRAFT IN FLIGHT AND IN THE 40- BY 80-FT WIND TUNNEL

Wayne Johnson*

Ames Research Center
and
Ames Directorate
U.S. Army Air Mobility R&D Laboratory

SUMMARY

Pretest predictions of the dynamic characteristics of the XV-15 tilting proprotor aircraft are presented. The data for the aircraft in flight includes: trim conditions, flight dynamics, gust response, aeroelastic stability, and wing response to control. The data for the aircraft in the Ames 40- by 80-ft wind tunnel includes aeroelastic stability, and the wing response to control. The calculations were made for pylon tilt angles of 0° (airplane mode), 0.1° (pylon unlocked), 30°, 60°, and 90° (helicopter mode).

INTRODUCTION

The NASA/Army XV-15 is a research aircraft intended to demonstrate the feasibility of the tilting proprotor configuration. The aircraft will be tested in the NASA/Ames 40- by 80-ft wind tunnel, and then in flight. A principal objective of the test program is to determine the aerelastic characteristics of the aircraft. This report documents the pretest predictions of the dynamics of the XV-15 aircraft in flight and in the wind tunnel.

The analysis on which these calculations were based is described in reference 1. The input data describing the aircraft were obtained from references 2 to 4; the rotor description is given in reference 5.

---

*Research Scientist, Large Scale Aerodynamics Branch, NASA-Ames Research Center

XV-15 IN FLIGHT

The dynamics characteristics of the XV-15 aircraft in flight were calculated as a function of forward speed for five pylon tilt angles: $\alpha_p = 0^\circ$ (airplane mode), 0.1° (pylon unlocked), 30°, 60°, and 90° (helicopter mode). The basic operating condition is trimmed level flight at a gross weight of 5900 kg; mid CG position; sea-level, standard day, and out of ground effect (the influences of altitude and ground effect are considered for certain cases). The rotor speed is 458 rpm for airplane mode ($\alpha_p = 0$), and 565 rpm for $\alpha_p = 0.1^\circ$ to 90°. The flap setting is zero for airplane mode, and $40/25^\circ$ for $\alpha_p = 0.1^\circ$ to 90° (see reference 2). Only symmetric trimmed flight conditions are considered, so the symmetric and antisymmetric motions of the aircraft are uncoupled.

The analysis includes the following degrees of freedom for the rotor: gimbal pitch and yaw, two elastic bending modes per blade, one rigid pitch mode per blade, and the rotor speed perturbation. It was established in reference 5 that this is an adequate model for proprotor dynamics. The rotor inflow perturbation is included (a quasistatic model for rotor unsteady aerodynamics, described in reference 1); its influence is small however for this aircraft, except for the in-ground-effect cases. The aircraft motions include three rigid body degrees of freedom (pitch, longitudinal velocity, and vertical velocity for symmetric dynamics, or roll, yaw, and lateral velocity for anti-symmetric dynamics); and four elastic modes -- fundamental wing vertical bending, chordwise bending, and torsion (all the modes below 10 Hz), and pylon yaw. The structural vibration mode shapes and frequencies were obtained from NASTRAN calculations supplied by the Bell Helicopter Company. A structural damping of 1% critical was assumed for all modes. The engine and transmission dynamics are modelled, including the rotor speed governor (for symmetric motions) and the interconnect shaft (for anti-symmetric motions). The trim calculation includes the effects of rotor-wing-tail aerodynamic interference (using an approximate

model described in reference 1). The dynamic characteristics were evaluated using the constant coefficient approximation for the rotor, which is an excellent approximation for the low advance ratios involved in tilting proprotor aircraft flight conditions (reference 5).

Figures 1 and 2 present the results for the XV-15 trim. The power required is for the two rotors only (figure 1). The cyclic stick position (δ_s, figure 2) is equivalent to rotor longitudinal cyclic pitch in helicopter mode ($\alpha_p = 90^\circ$); the control system schedules cyclic with pylon angle so in general the rotor longitudinal cyclic pitch equals $\delta_s * \sin\alpha_p$ (reference 4). The elevator angle is $1.93\,\delta_s$ (all pylon tilt angles). The effect of aerodynamic interference in cruise ($\alpha_p = 0$) is due to the wing downwash at the horizontal tail. The effect of aerodynamic interference in helicopter mode ($\alpha_p = 90^\circ$) is due to rotor-induced wing stall below 70 knots.

Figures 3 to 7 give the period and time to half amplitude for the XV-15 flight dynamics modes. The principal influence of aerodynamic interference is in helicopter mode, due to stalling of the horizontal tail (figures 3 and 4). The model used assumes that there are no perturbation aerodynamic forces from the tail when it is stalled. The aircraft flight dynamics were also calculated without the rotor speed governor operating. The principal influence observed was on the phugoid damping in cruise, which can even be unstable, due to the reduced longitudinal damping (C_{X_u}) from the rotors when the governor is inoperative. The governor was also found to have a significant effect on the pitch and vertical modes in helicopter flight.

A quasistatic rotor dynamics model is frequently used for tiltrotor flight dynamics analyses. Table 1 compares the roots obtained using the complete dynamics model (case 1) and using the approximate quasistatic model (for all degrees of freedom except the rigid body motions, case 2), for the XV-15 in hover and cruise. The quasistatic model is very good for the cases considered. Of greater importance are the degrees of freedom included in the quasistatic model. Case 3 in Table 1 only includes the

rotor flapping and rotational speed degrees of freedom; there are significant differences in the roots with this limited model.

The influence of ground effect on the XV-15 dynamics in hover is shown in figure 8 (root loci) and Table 2 (period and time to half amplitude). At h = 1.5m (approximately) the aircraft gear contacts the ground. Ground effect introduces a positive spring on the vertical motions (figure 8a). Figure 8b shows the influence of the negative roll spring due to ground effect (modelled using data from reference 4).

Figures 9 and 10 present the gust response of the XV-15 aircraft in cruise flight ($\alpha_p = 0$). The rms acceleration at the pilot station is given, for unit rms gust velocity. A gust spectrum characteristic of low altitude flight was used (see reference 6). An rms gust strength of σ_G = 2 m/sec is typical of clear air turbulence (CAT), and σ_G = 6 m/sec for thunderstorms. Thus for V = 280 knots, the 3σ vibration level in CAT is about .9g vertically, .55g longitudinally, and .65g laterally. There is little influence of the SAS (attitude hold on or off) on the gust response. The quasistatic model is not satisfactory for calculating the gust response, due to the participation of the rotor and aircraft elastic modes.

Figure 11 shows the natural frequencies of the aircraft structural vibration modes (NASTRAN calculations). Figures 12 and 13 present the aeroelastic stability of the XV-15 aircraft in cruise mode flight ($\alpha_p = 0$) at sea level. The predicted stability boundary is at V = 300 knots. Note that the aircraft vibration mode shapes are quite complex, particularly for anti-symmetric motions, so the designation of the modes as vertical bending, chordwise bending, or torsion does not imply uncoupled motions. Figures 14 to 17 present the aeroelastic stability for pylon angles $\alpha_p = 0.1^\circ$, 30°, 60°, and 90° respectively. There is little effect of aerodynamic interference, the rotor speed governor, or the SAS on the dynamic stability. Figure 18 presents the aeroelastic stability of the XV-15 in cruise flight at an altitude of 3800m. The predicted stability boundary is at V = 340 knots.

XV-15 IN THE WIND TUNNEL

The dynamic characteristics were also calculated for the XV-15 aircraft in the Ames 40- by 80-ft wind tunnel. The analysis used basically the same model as described above for the free flight case. Figure 19 shows the natural frequencies of the aircraft structural vibration, including the strut and balance frame modes. The vibration modes and frequencies for the aircraft in the wind tunnel were calculated by coupling the NASTRAN results for the aircraft free vibration (figure 11) with the balance and strut model described in reference 7. The 15-ft strut/33-in tip combination was considered. The stiffness for this combination was estimated based on shake test results for other strut/tip combinations. The balance motions have little role in the aircraft dynamics. However the support system has a significant effect on the frequencies compared to free vibration, and it adds symmetric and anti-symmetric strut modes to the dynamic system.

Figures 20 and 21 present the aeroelastic stability of the XV-15 aircraft in the wind tunnel at $\alpha_p = 0^\circ$ (airplane mode). The predicted stability boundary is V = 260 knots, beyond the speed capability of the tunnel. Figure 22 to 25 present the aeroelastic stability for pylon angles of $\alpha_p = 0.1^\circ$, 30°, 60°, and 90° respectively.

WING RESPONSE TO CONTROL

The XV-15 aircraft will be tested, in flight and in the wind tunnel, using the right wing flaperon and the right rotor collective pitch to excite the aeroelastic modes. Figure 26 shows the transfer functions (magnitude and phase) of the wing bending response to control for the aircraft in cruise flight at V = 180 knots. The abscissa is the excitation frequency, normalized by rotor rotational speed (i.e. per rev). The wing bending (at the mid-span) is considered to eliminate the rigid body motions from the response at low frequency. Figure 27 shows the transfer functions of the wing tip displacement response to control for the aircraft in the wind tunnel (V = 180 knots, $\alpha_p = 0$).

CONCLUDING REMARKS

This report has presented the pretest predictions of the aeroelastic characteristics of the XV-15 aircraft for the wind tunnel and flight tests. These results may be updated as more information about the aircraft properties becomes available, such as from shake tests of the airframe. These predictions provide a guide for the testing of the XV-15, and correspondingly correlation with the experimental data will further validate the proprotor analytical model, and the understanding of tilting proprotor aircraft dynamics upon which the model is based.

REFERENCES

1. Johnson, Wayne, "Aeroelastic Analysis for Rotorcraft in Flight or in a Wind Tunnel," NASA TN-D, in preparation

2. Tilt Rotor Project Office Staff, "Tilt Rotor Research Aircraft Familiarization Document," NASA TM X-62407, January 1975

3. Bell Helicopter Company, "V/STOL Tilt Rotor Research Aircraft, Vol 1-4," Reports 301-199-001 to -004, 1975

4. Harendra, P.B.; Joglekar, M.J.; Gaffey, T.M.; and Marr, R.L.: "A Mathematical Model for Real Time Flight Simulation of the Bell Model 301 Tilt Rotor Research Aircraft," NASA CR 114614, April 1973

5. Johnson, Wayne, "Analytical Modeling Requirements for Tilting Proprotor Aircraft Dynamics," NASA TN D-8013, July 1975

6. Johnson, Wayne, "Optimal Control Alleviation of Tilting Proprotor Gust Response," NASA TM X-62494, October 1975

7. Johnson, Wayne, "Analytical Models for Rotor Test Module, Strut, and Balance Frame Dynamics in the40- by 80-ft Wind Tunnel," NASA TM X- June 1976

Table 1. XV-15 aircraft in flight, quasistatic approximation for rotor dynamics

A. Hover

	longitudinal modes				lateral modes			
	oscillatory		pitch	vert.	oscillatory		roll	yaw
	T	t_2	$t_{\frac{1}{2}}$	$t_{\frac{1}{2}}$	T	t_2	$t_{\frac{1}{2}}$	$t_{\frac{1}{2}}$
1. Complete dynamics model	10.97	2.372	1.003	2.639	22.51	18.79	.8754	7.258
2. Quasistatic dynamics	10.97	2.370	1.001	2.650	22.54	18.25	.8742	7.254
3. Quasistatic, with only rigid body, rotor flap, and rotor speed degrees of freedom	11.21	2.366	1.043	1.997	24.28	47.69	.6346	7.671

B. Cruise (200 knots)

	longitudinal modes				lateral modes			
	short period		phugoid		dutch roll		roll	sprial
	T	$t_{\frac{1}{2}}$	T	$t_{\frac{1}{2}}$	T	$t_{\frac{1}{2}}$	$t_{\frac{1}{2}}$	$t_{\frac{1}{2}}$
1. Complete dynamics model	2.338	.3901	26.39	29.67	2.917	.8131	.6404	11.68
2. Quasistatic dynamics	2.400	.3248	26.43	31.54	2.920	.8480	.6033	11.66
3. Quasistatic, with only rigid body, rotor flap, and rotor speed degrees of freedom	2.275	.3278	27.83	31.34	2.853	.7814	.7122	10.43

Table 2. Influence of ground effect on XV-15 hover flight dynamics.

A. Longitudinal modes

altitude CG above ground	oscillatory T	oscillatory t_2	pitch $t_{\frac{1}{2}}$	vertical $t_{\frac{1}{2}}$
∞ (OGE)	10.98	2.320	1.018	2.639
7.6 m	10.97	2.344	1.006	3.342, 13.58
6.9	10.97	2.345	1.005	3.779, 9.353
6.1	10.97	2.346	1.005	T = 166.9, $t_{\frac{1}{2}}$ = 5.407
5.3	10.97	2.349	1.005	71.01 5.436
4.6	10.97	2.352	1.004	47.34 5.492
3.8	10.97	2.356	1.003	34.47 5.581
3.0	10.98	2.400	.995	25.69 5.707
2.3	10.98	2.433	.982	19.09 5.973
1.5	10.98	2.459	.979	13.83 6.573

B. Lateral modes

altitude CG above ground	oscillatory T	oscillatory t_2	roll $t_{\frac{1}{2}}$	yaw $t_{\frac{1}{2}}$
∞ (OGE)	22.51	18.79	.8754	7.258
7.6 m	39.04	4.483	.6736	7.373
6.9	t_2 = 6.417	t_2 = 2.054	.5943	7.420
6.1	12.55	1.402	.5452	7.453
5.3	18.31	1.201	.5185	7.480
4.6	20.31	1.158	.5118	7.496
3.8	15.86	1.269	.5290	7.492
3.0	7.196	1.911	.5884	7.196
2.3	T = 25.58	t_2 = 8.664	.7915	7.412
1.5	T = 9.800	$t_{\frac{1}{2}}$ = 2.573	4.178	7.054

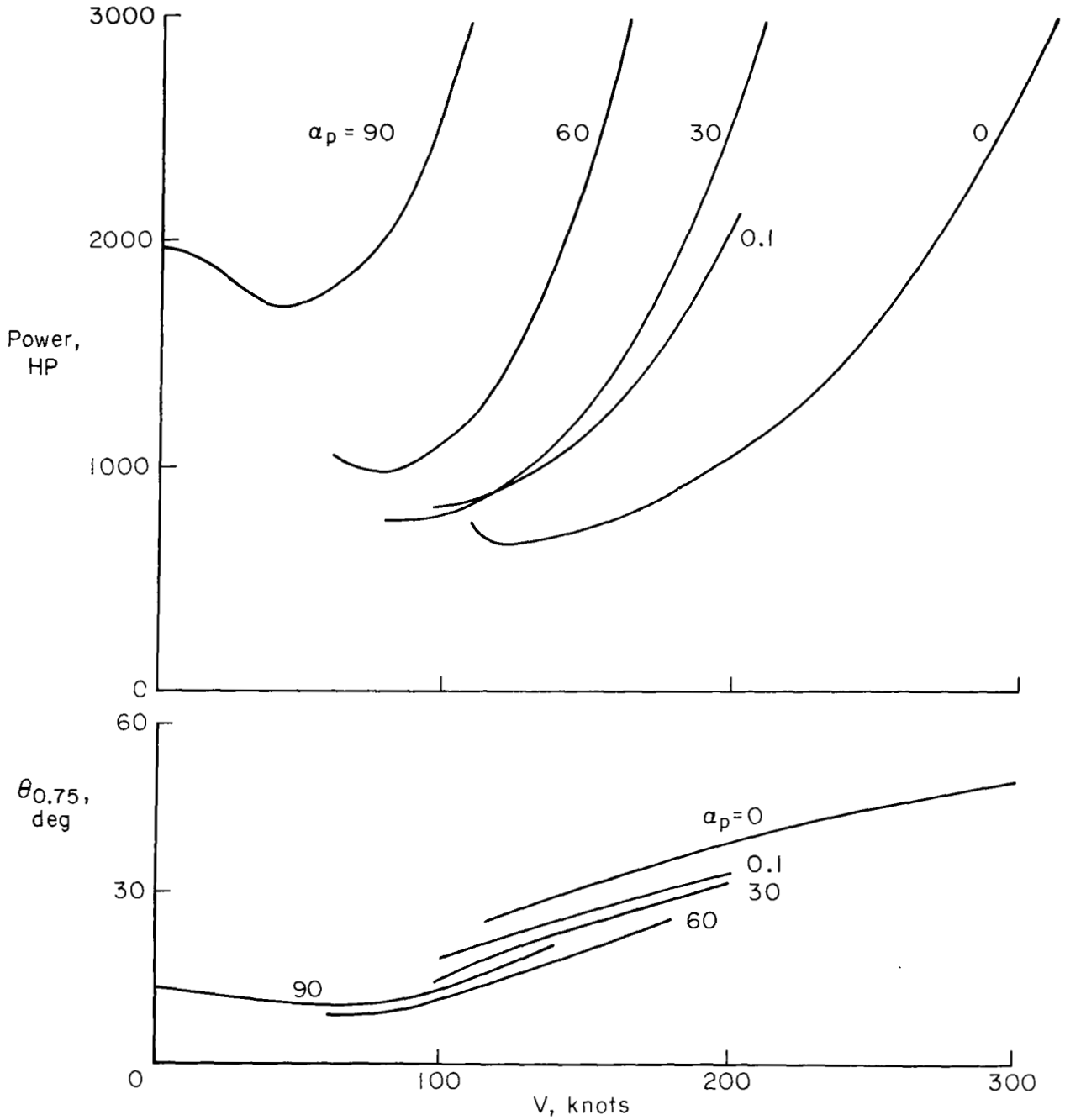

Figure 1. XV-15 aircraft in flight, sea level trim: power required and rotor collective pitch. (Note for $\alpha_p = 0.1^o$, the aircraft is in airplane configuration, but at high rpm and with flaps down.)

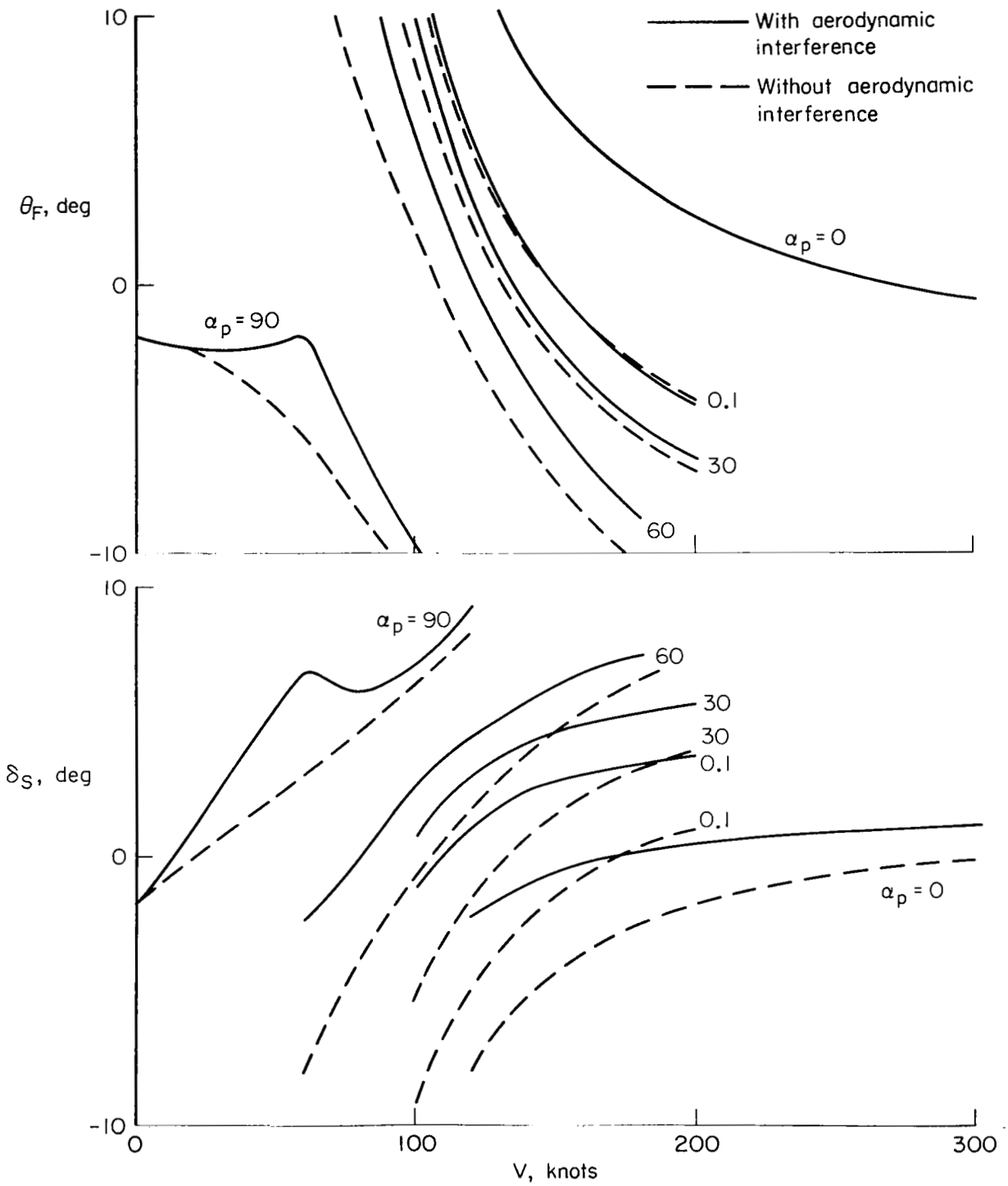

Figure 2. XV-15 aircraft in flight, sea level trim: aircraft pitch angle θ_F and longitudinal cyclic stick position δ_s.

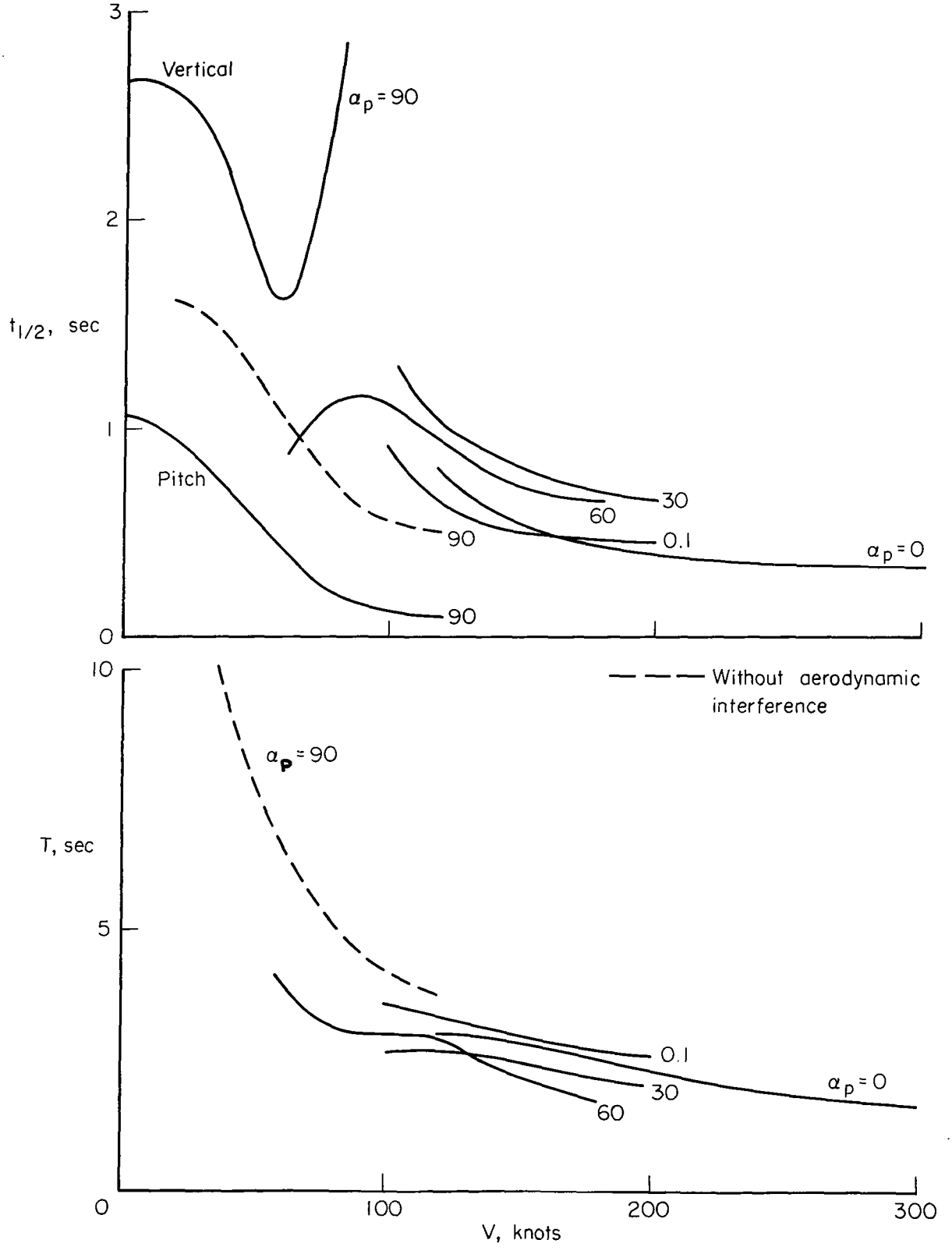

Figure 3. XV-15 aircraft sea level flight dynamics: short period mode period and time to half amplitude.

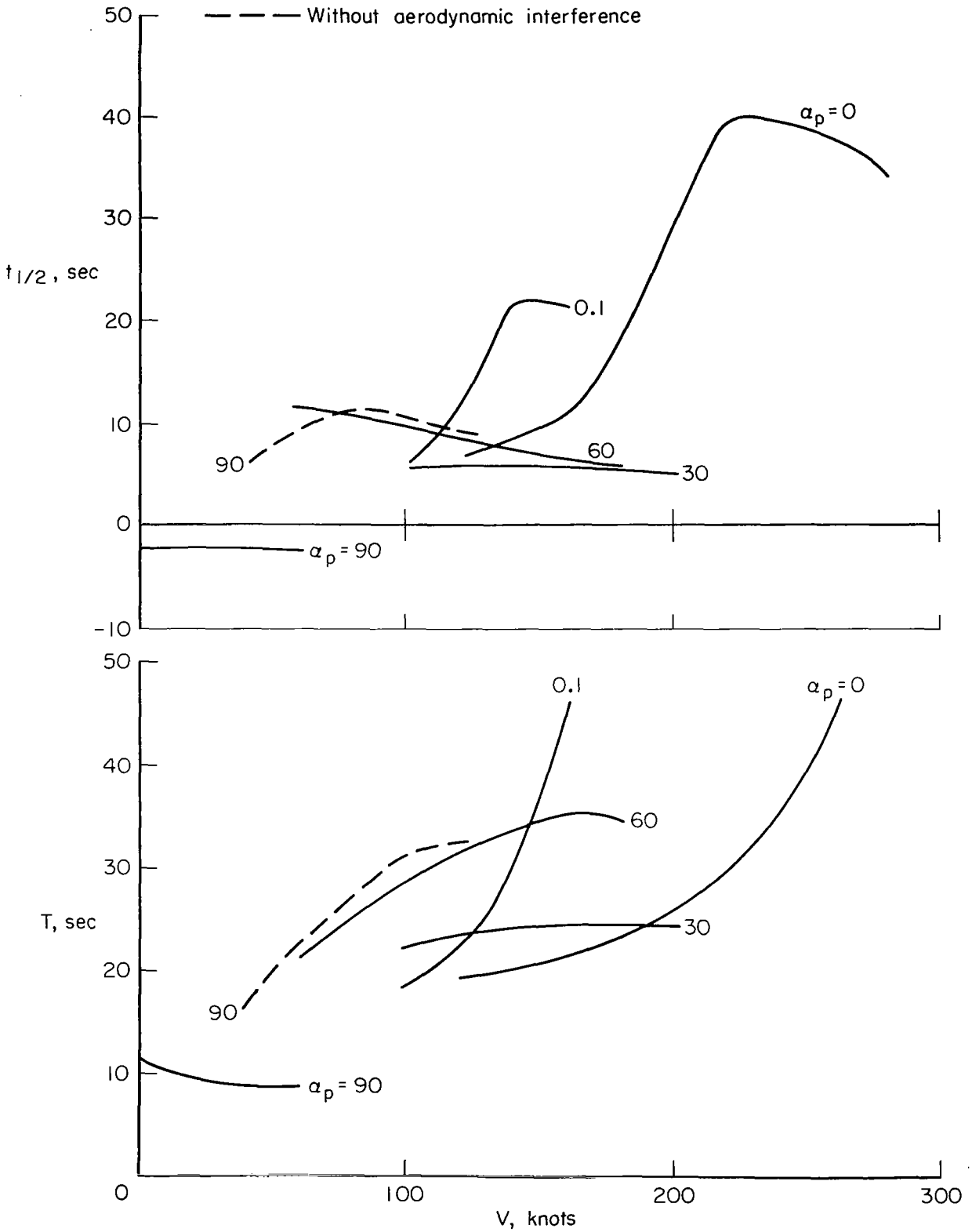

Figure 4. XV-15 aircraft sea level flight dynamics: phugoid mode period and time to half amplitude.

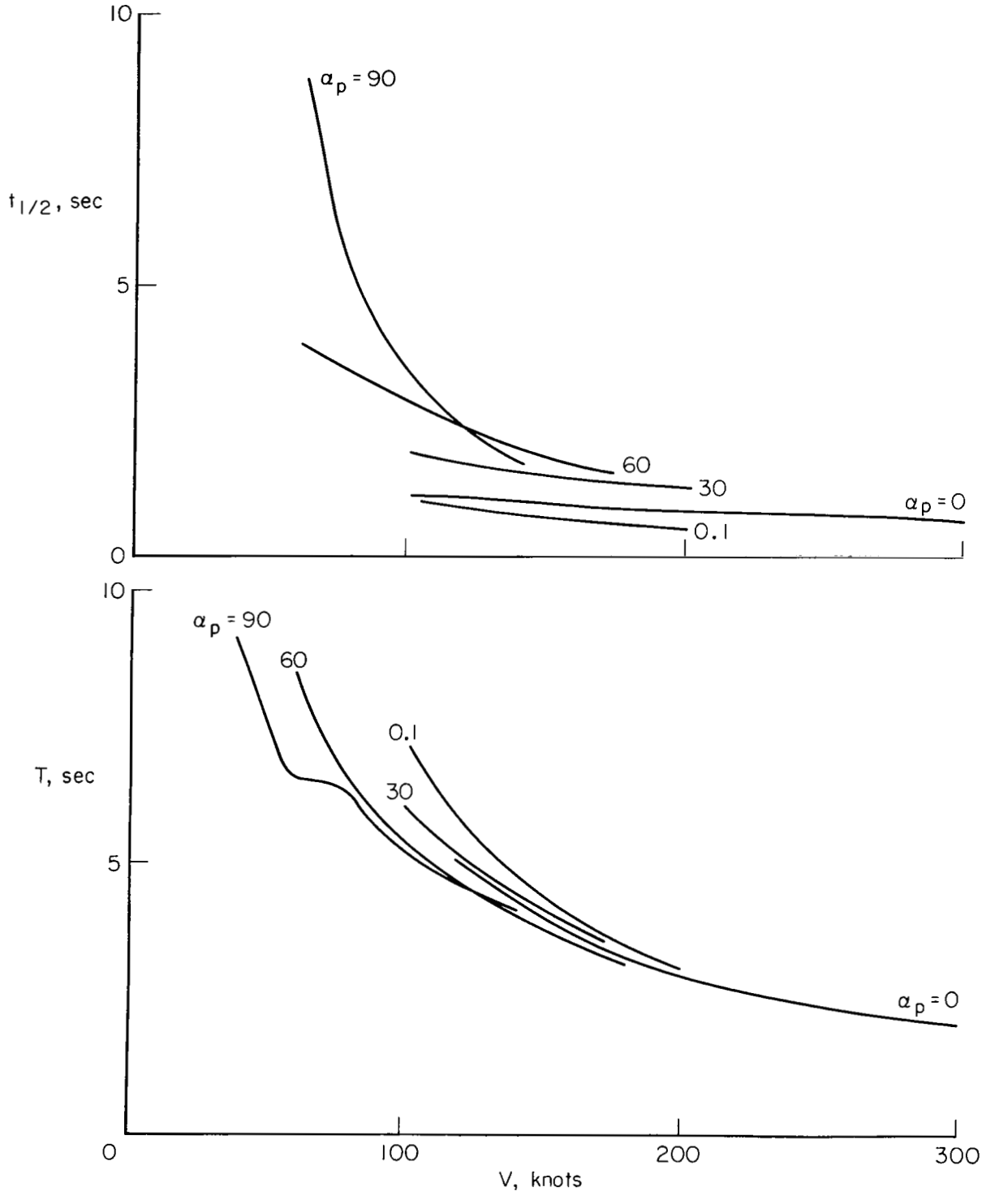

Figure 5. XV-15 aircraft sea level flight dynamics: dutch roll mode period and time to half amplitude.

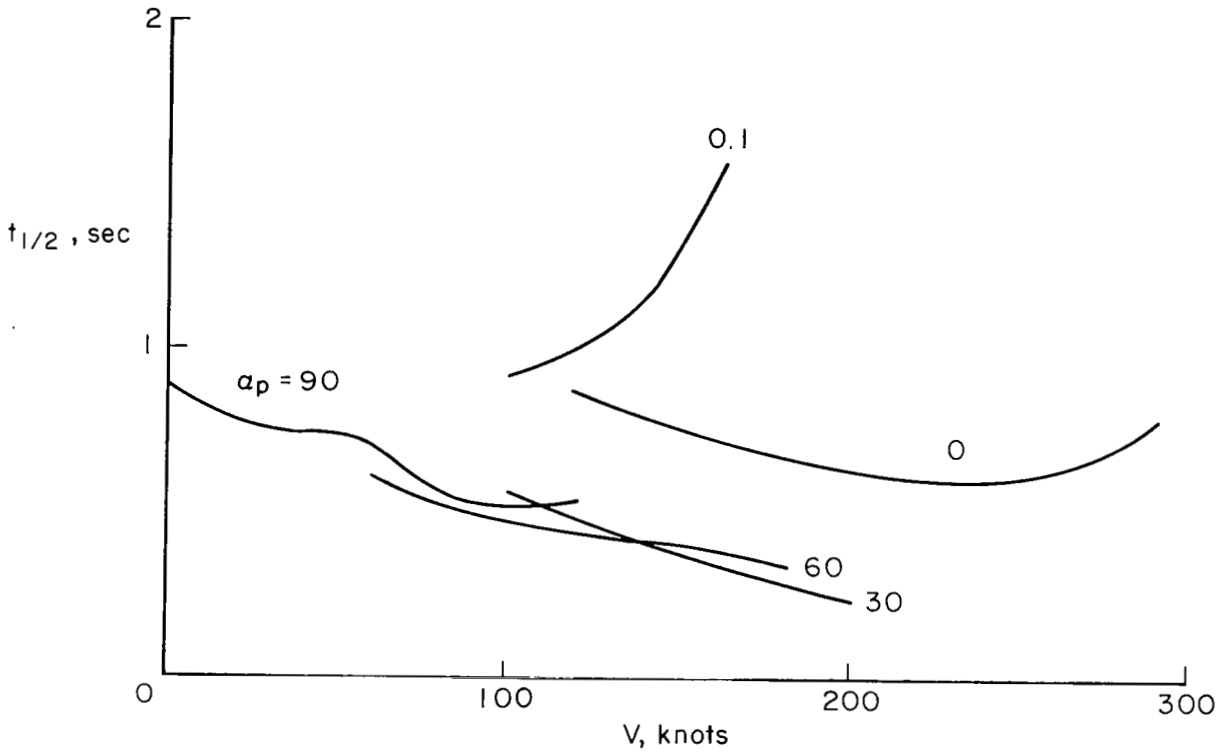

Figure 6. XV-15 aircraft sea level flight dynamics: roll mode time to half amplitude.

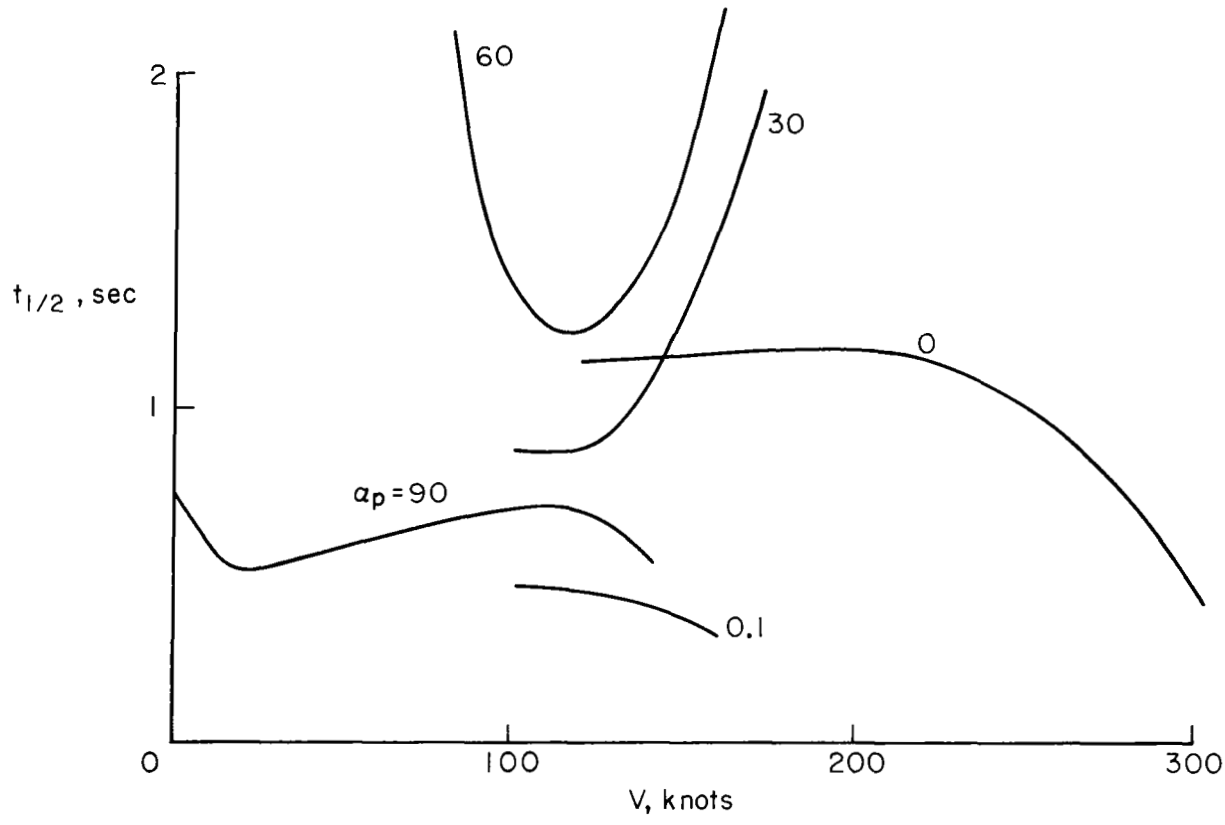

Figure 7. XV-15 aircraft sea level flight dynamics: yaw/spiral mode time to half amplitude.

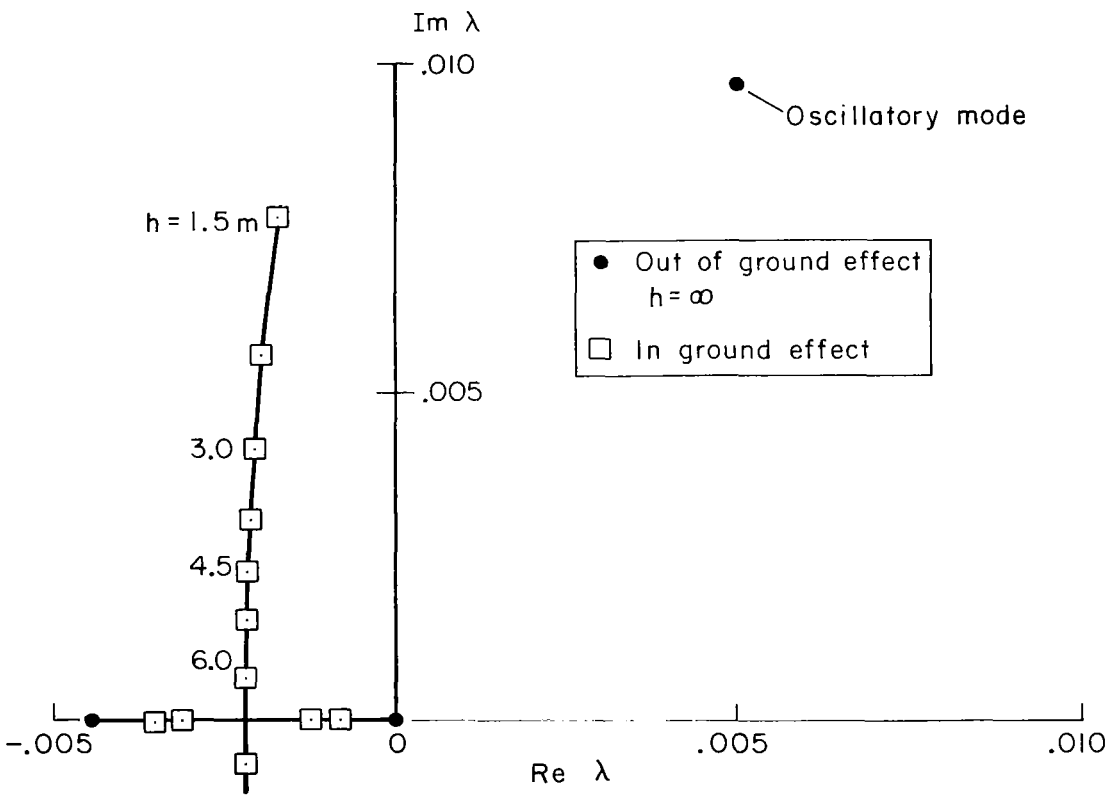

(a) Longitudinal roots -- vertical and oscillatory modes.

Figure 8. XV-15 aircraft flight dynamics for hovering in ground effect; root loci for altitude of CG above ground from infinity (out of ground effect) to h = 1.5m.

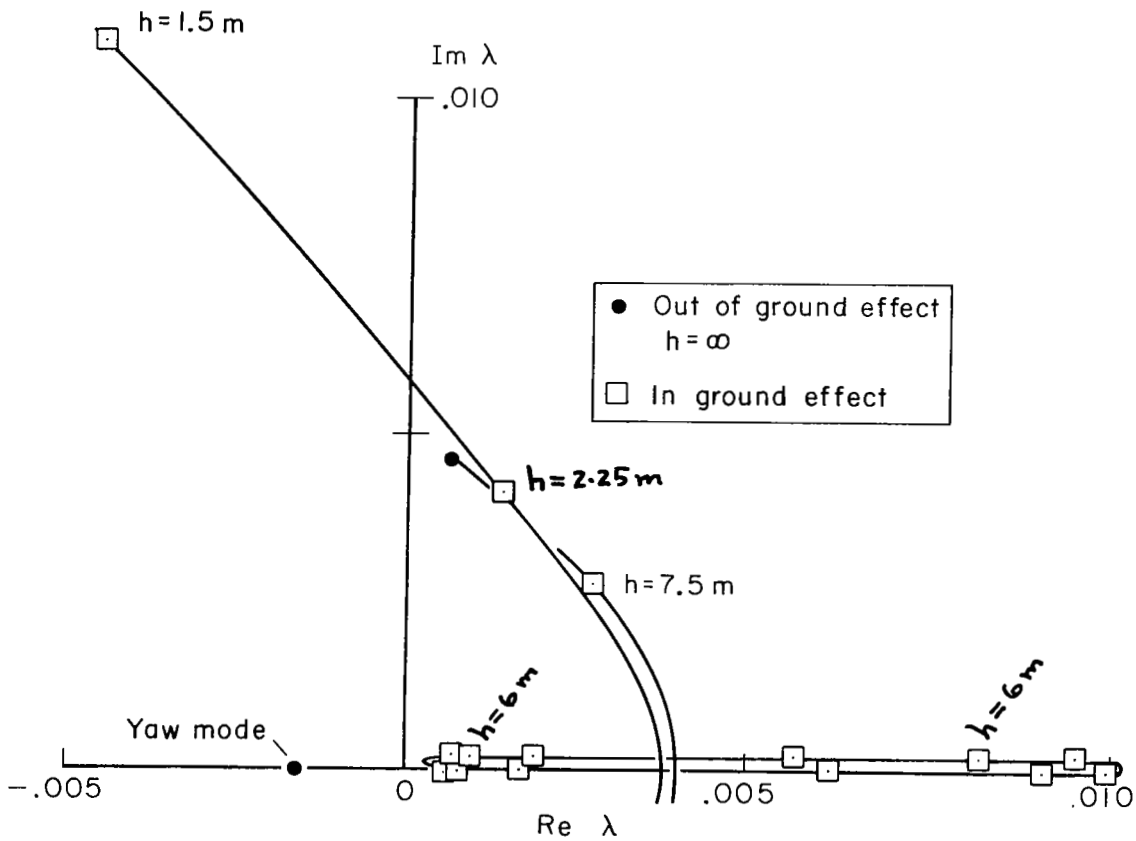

(b) Lateral roots -- yaw and oscillatory modes.

Figure 8. Concluded.

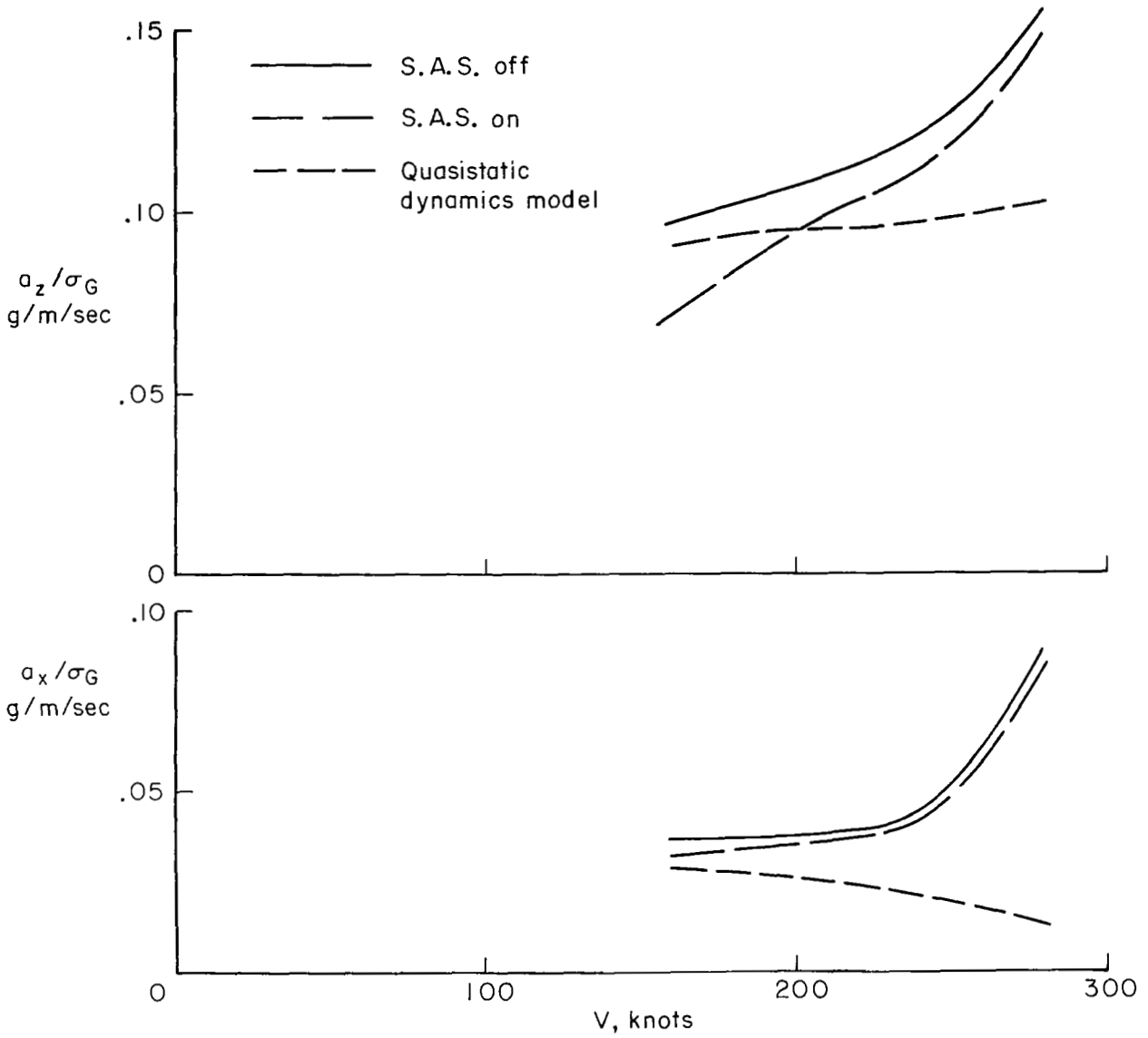

Figure 9. XV-15 aircraft rms gust response at pilot station in sea level cruise flight ($\alpha_\rho = 0$). Vertical (a_z) and longitudinal (a_x) acceleration response to combined vertical and longitudinal gusts. (See reference 4 for the SAS model.)

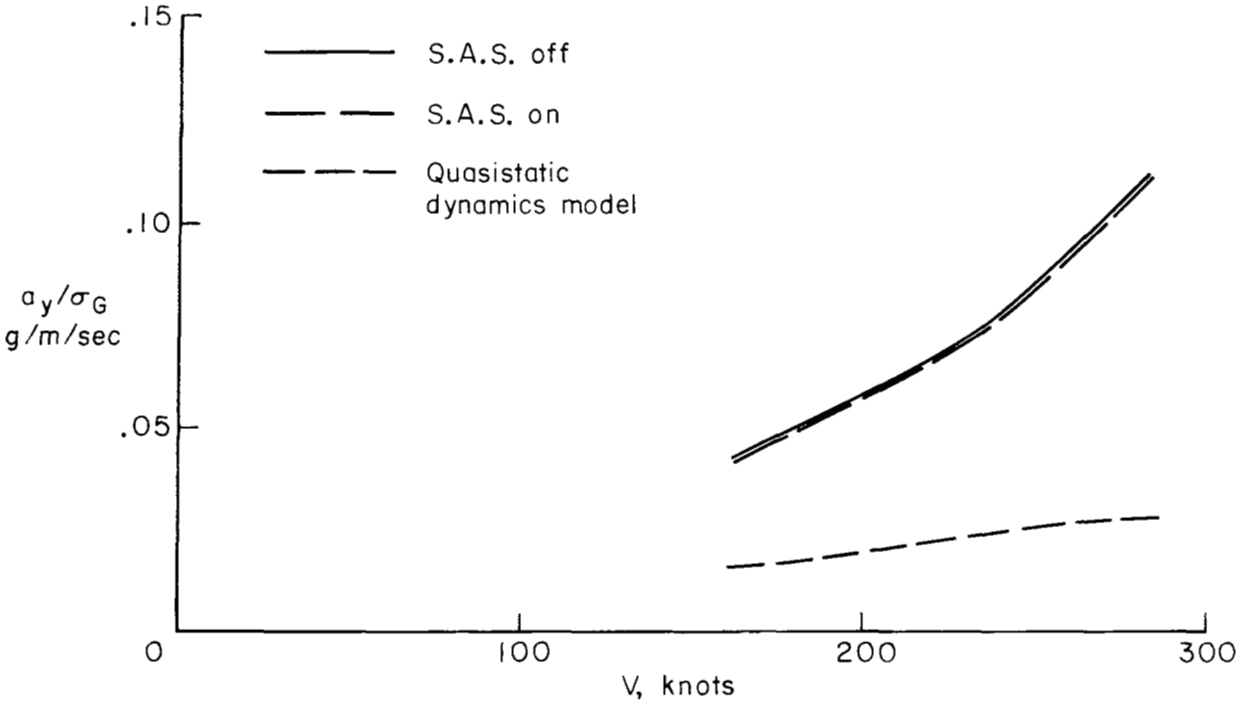

Figure 10. XV-15 aircraft rms gust response at pilot station in sea level cruise flight ($\alpha_p = 0$). Lateral acceleration (a_y) response to lateral gusts. (See reference 4 for the SAS model.)

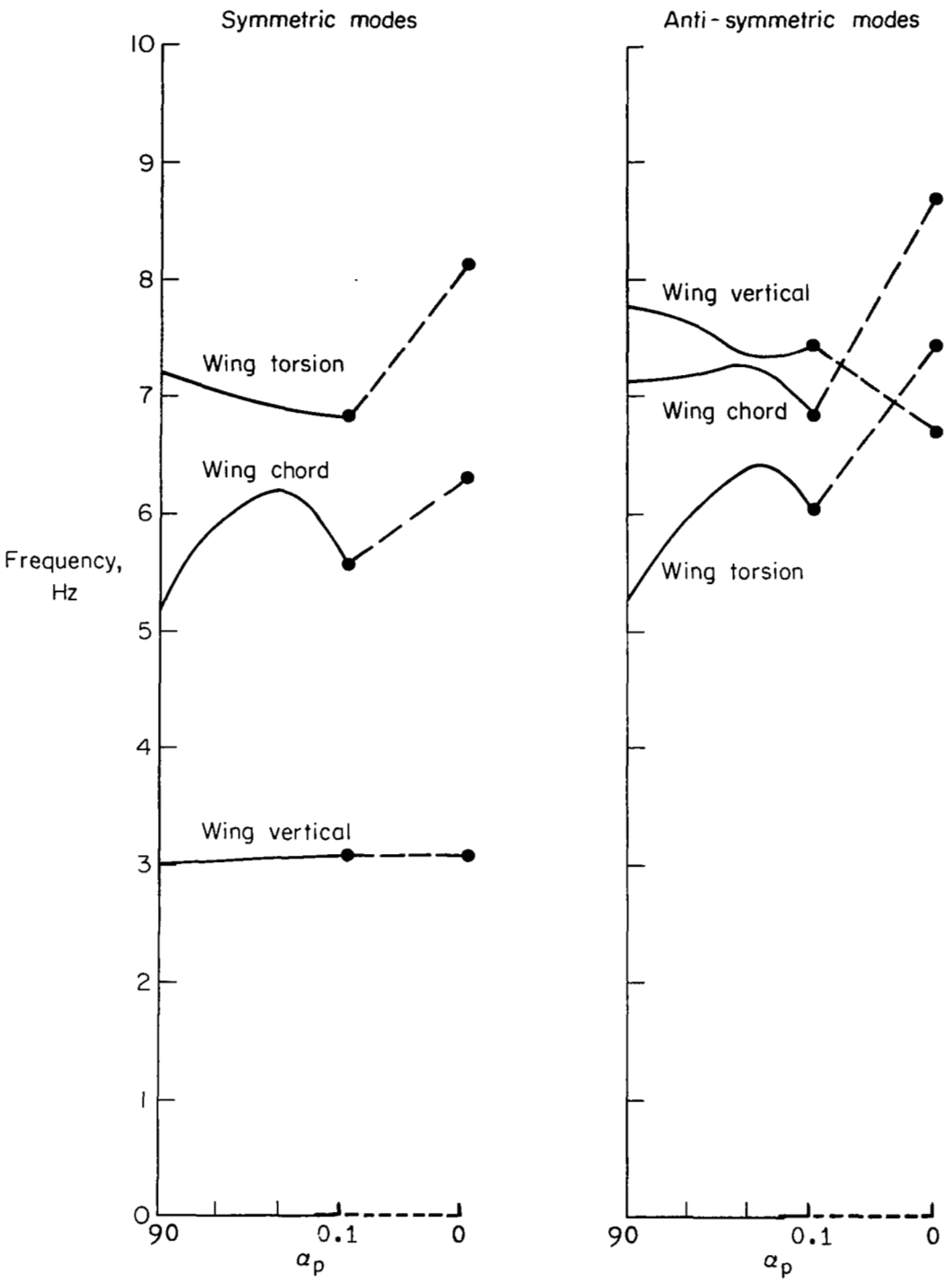

Figure 11. XV-15 aircraft in flight, natural frequencies of the structural vibration modes ($\alpha_p = 0.1$ is airplane mode with pylon unlocked; $\alpha_p = 0$ is pylon locked).

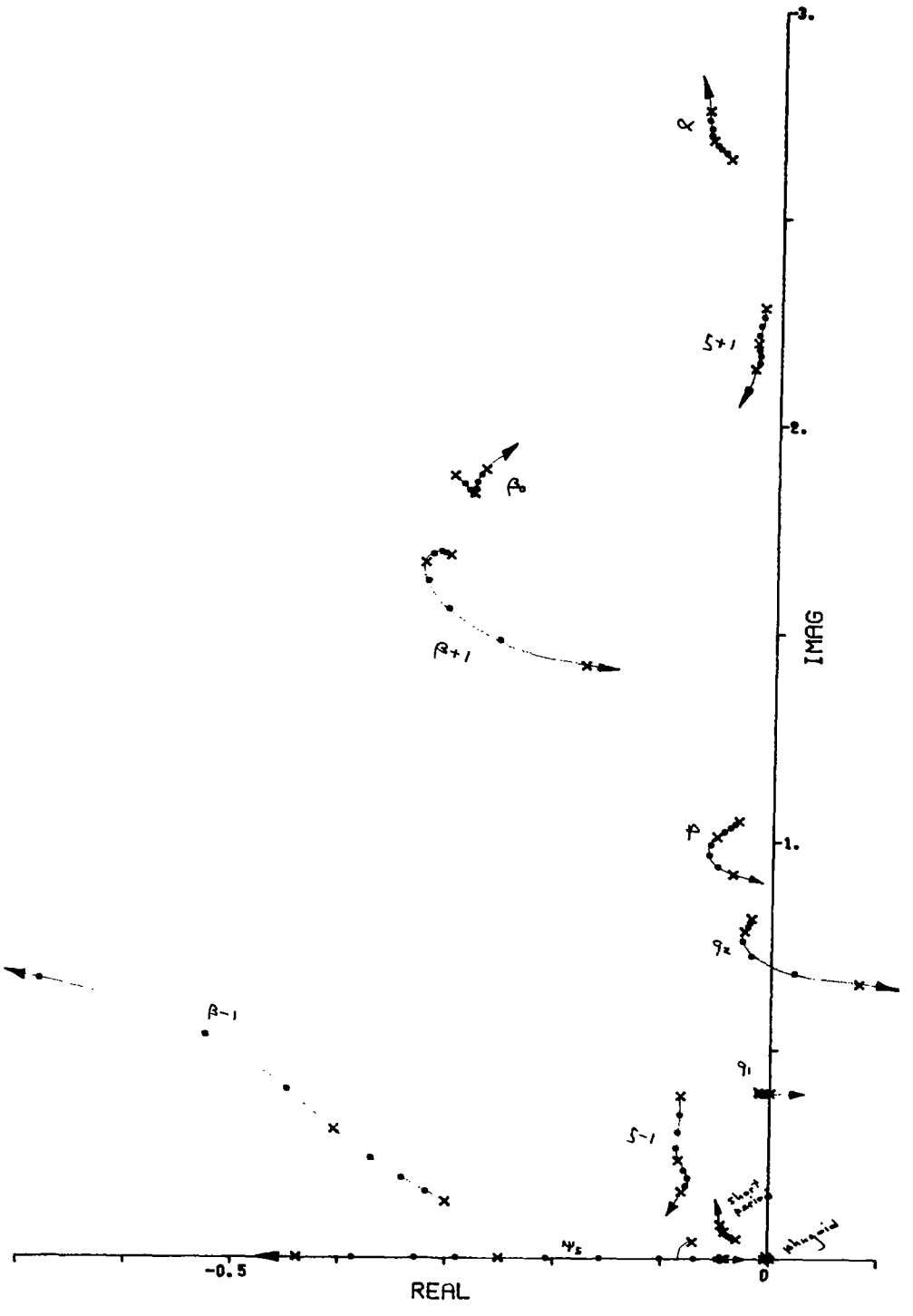

(a) Symmetric modes

Figure 12. XV-15 aircraft aeroelastic stability in flight, root locus for V = 160 to 320 knots (ΔV = 20 knots). Sea level cruise flight, α_p = 0.

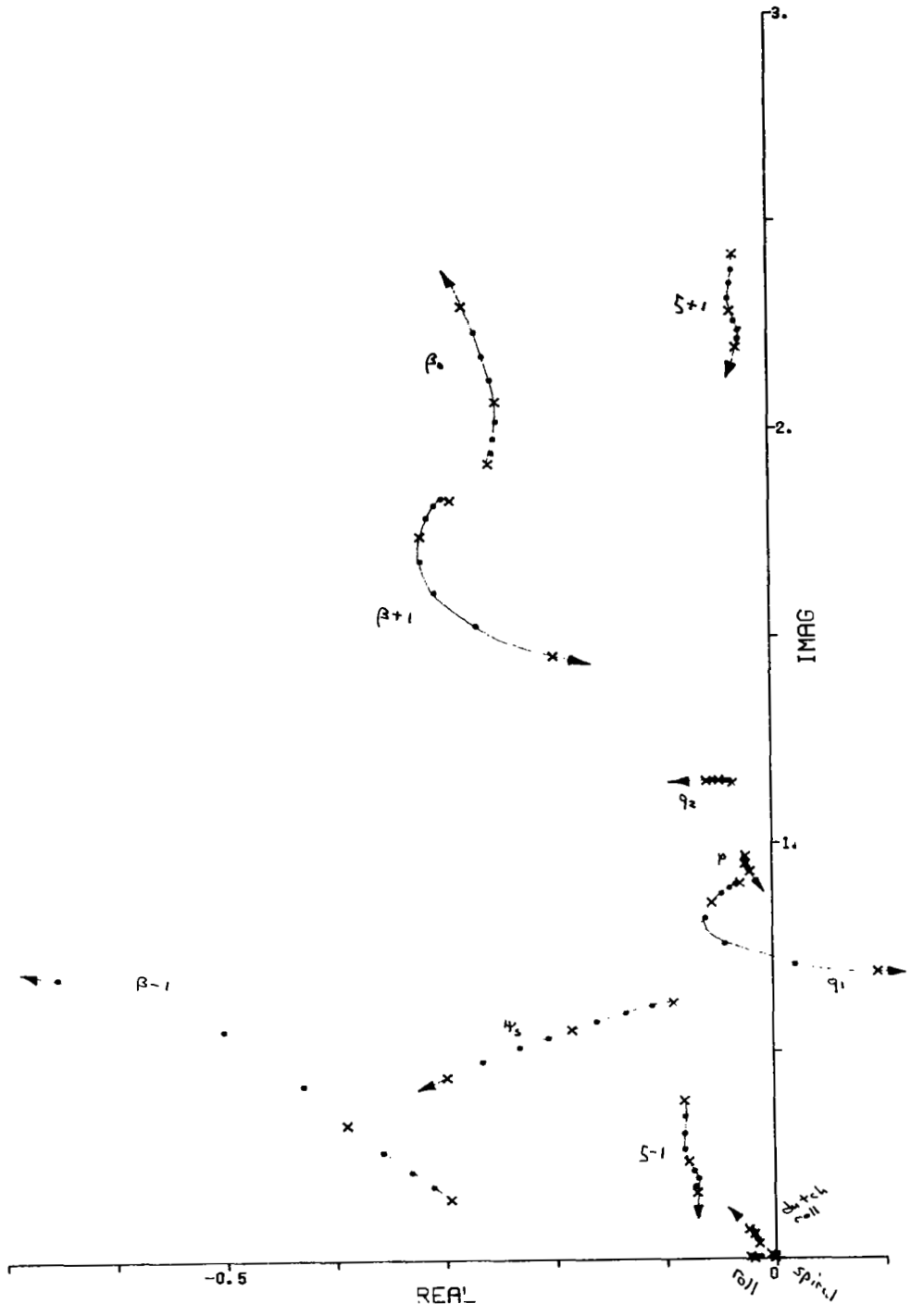

(b) Anti-symmetric modes

Figure 12. Concluded

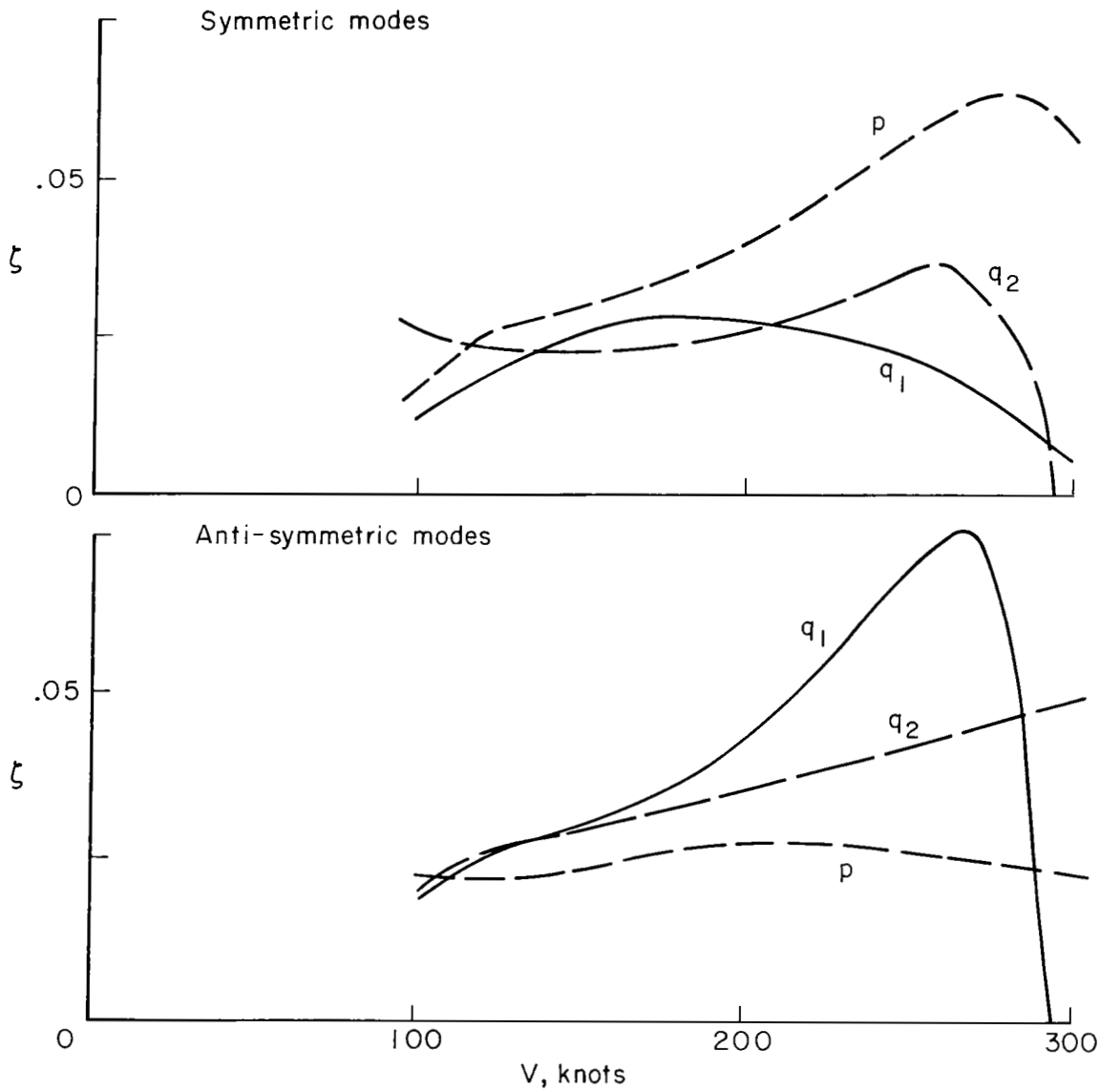

Figure 13. XV-15 aircraft aeroelastic stability in sea level flight: damping ratio for $\alpha_p = 0$ (airplane mode).

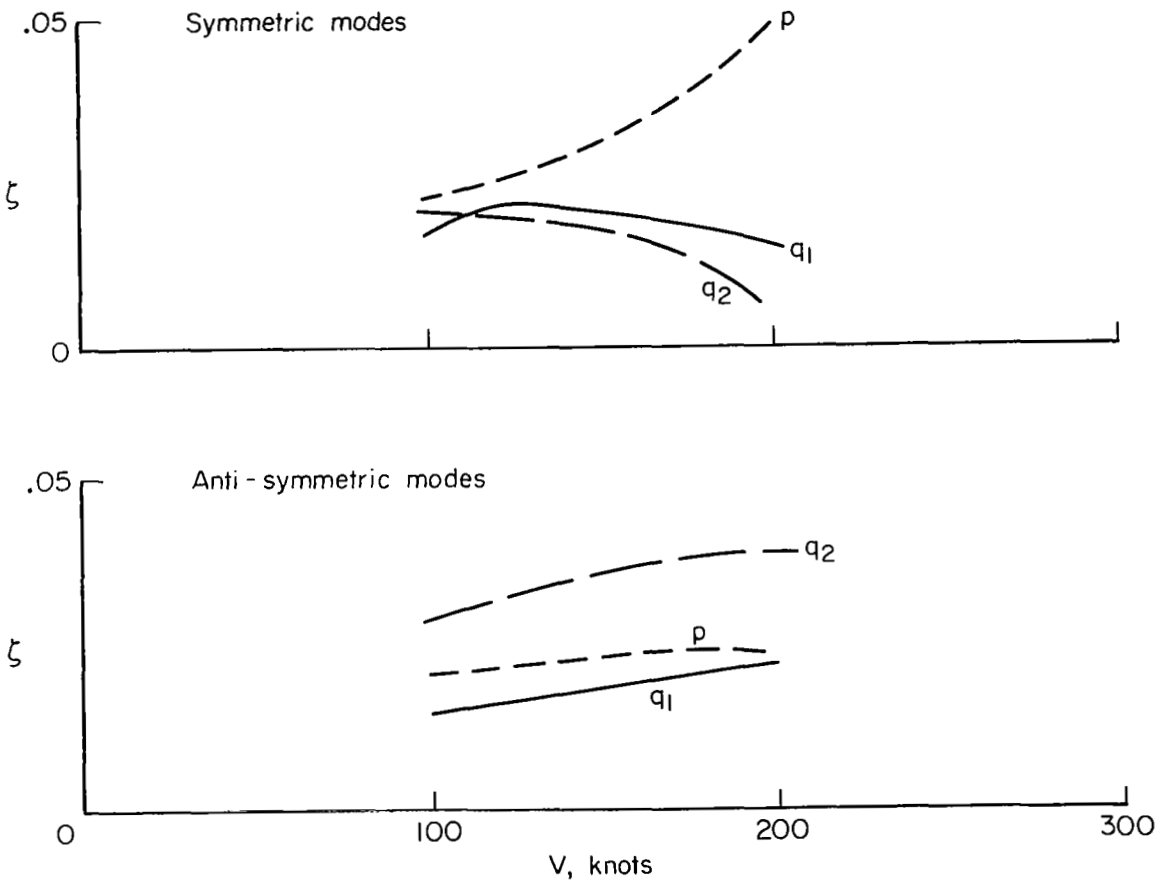

Figure 14. XV-15 aircraft aeroelastic stability in sea level flight: damping ratio for $\alpha_p = 0.1^o$ (pylon unlocked).

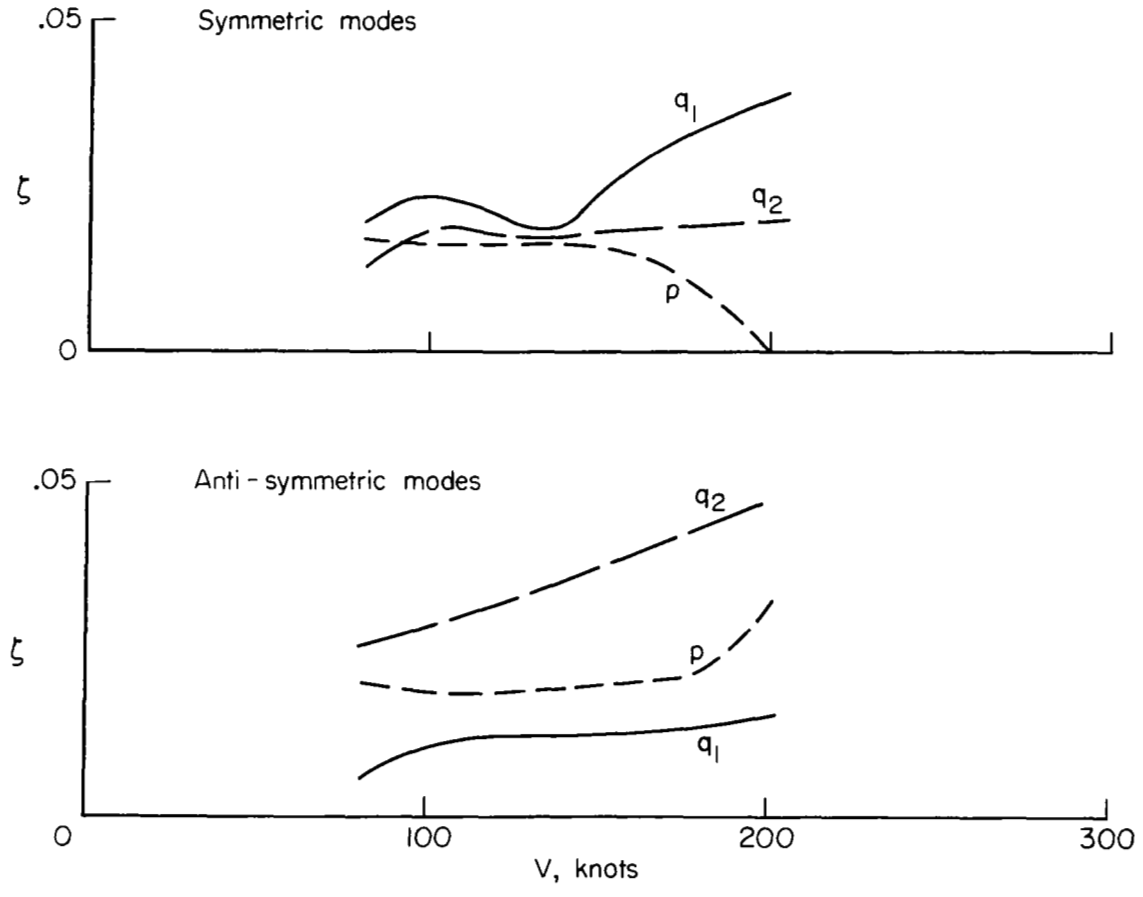

Figure 15. XV-15 aircraft aeroelastic stability in sea level flight: damping ratio for $\alpha_\rho = 30^\circ$.

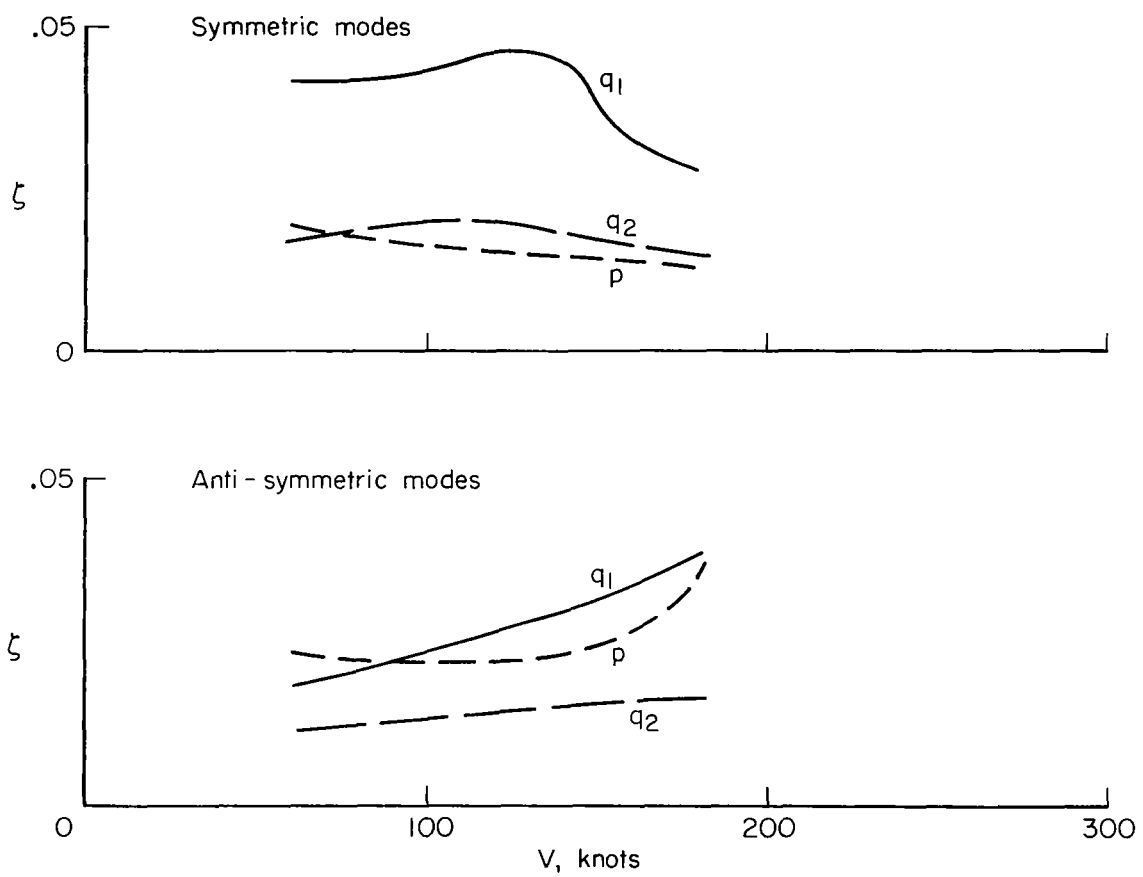

Figure 16. XV-15 aircraft aeroelastic stability in sea level flight: damping ratio for $\alpha_p = 60^\circ$.

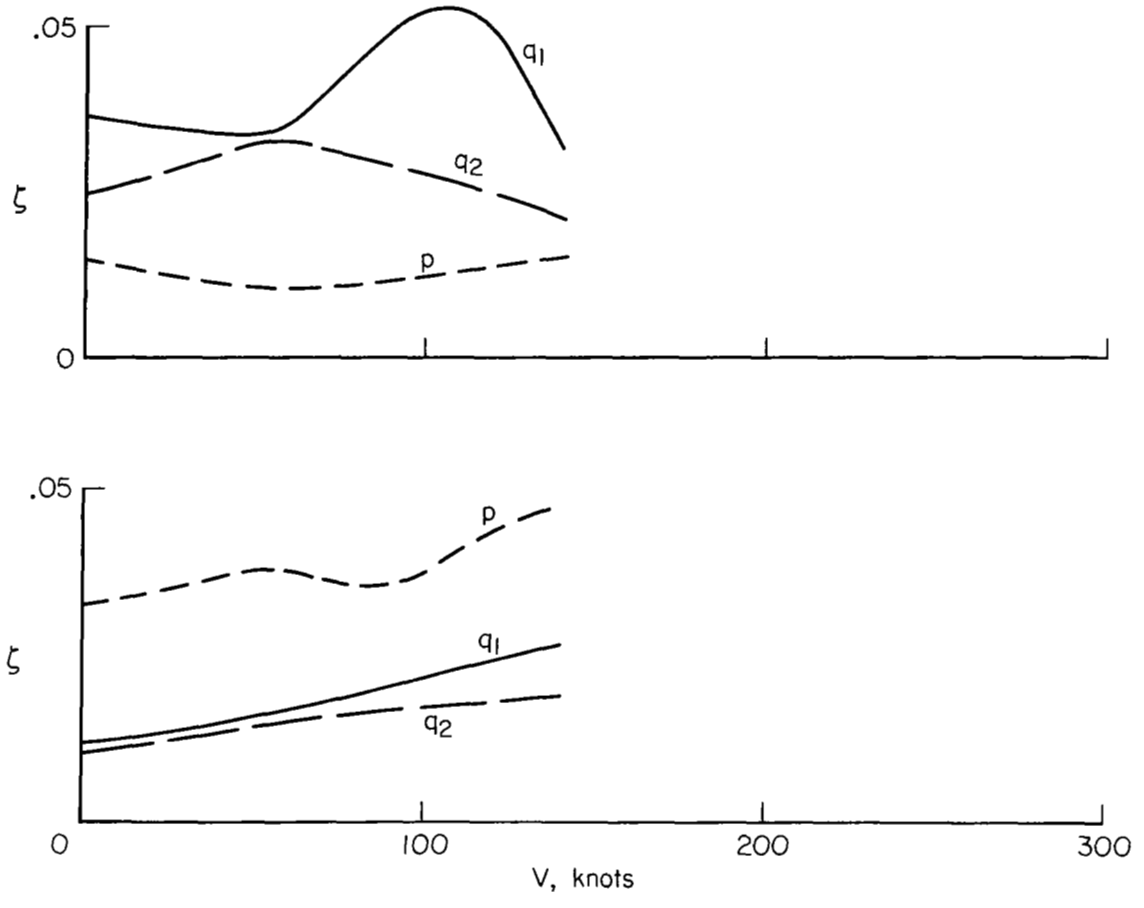

Figure 17. XV-15 aircraft aeroelastic stability in sea level flight: damping ratio for $\alpha_p = 90^o$ (helicopter mode).

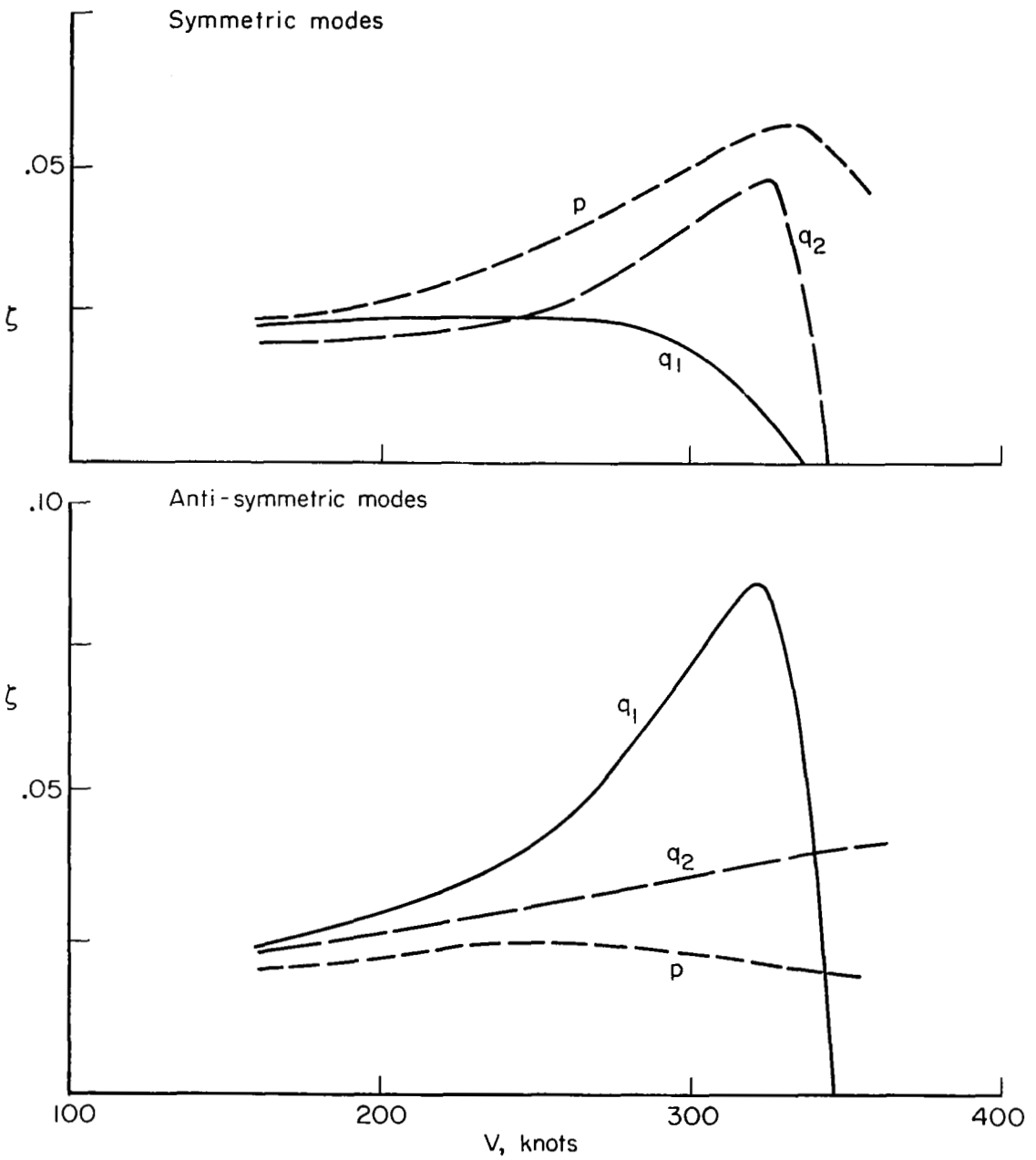

Figure 18. XV-15 aircraft aeroelastic stability in flight at 3800m altitude: damping ratio for $\alpha_p = 0$ (airplane mode).

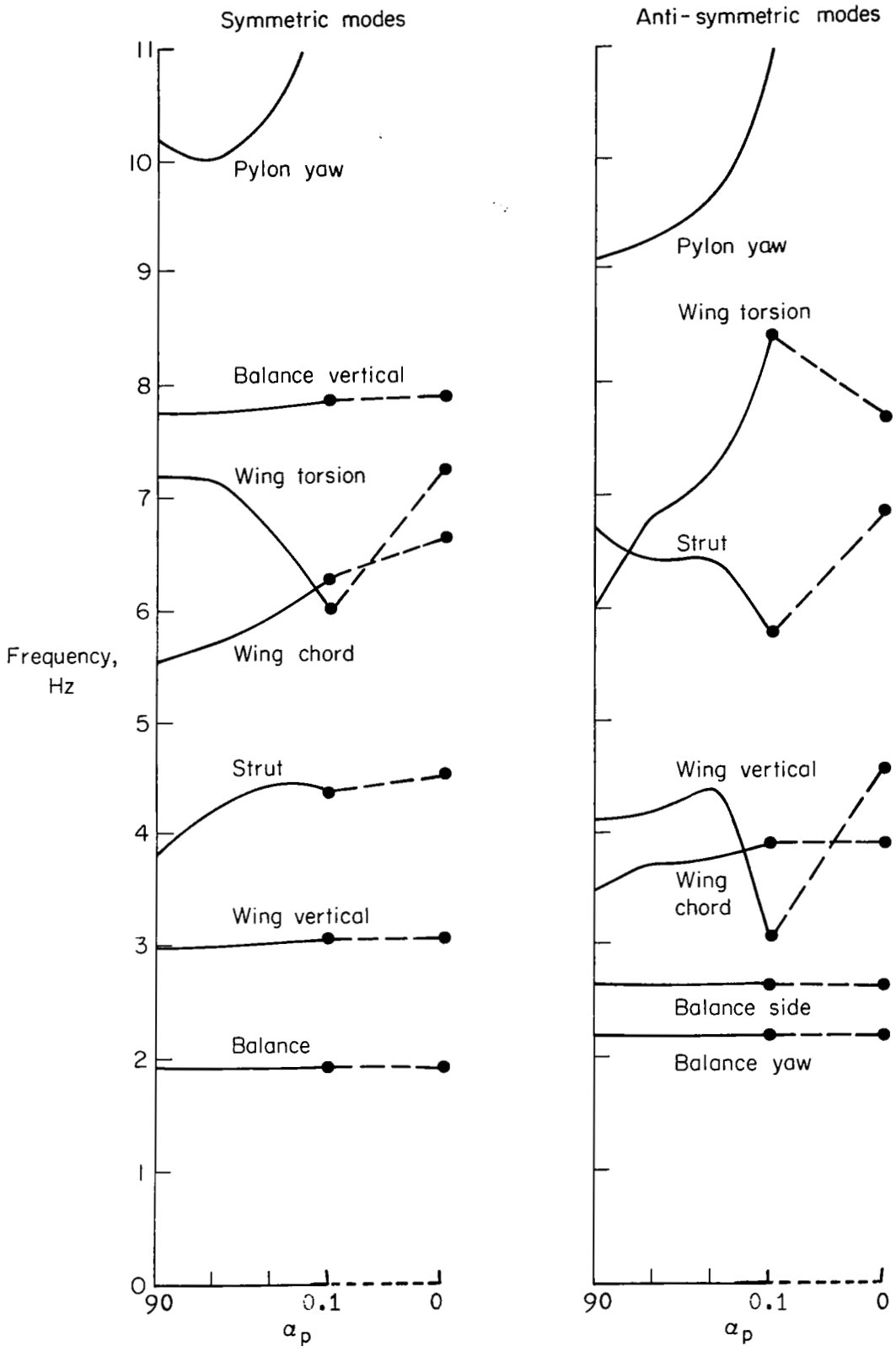

Figure 19. XV-15 aircraft in the wind tunnel, natural frequencies of the structural vibration modes.

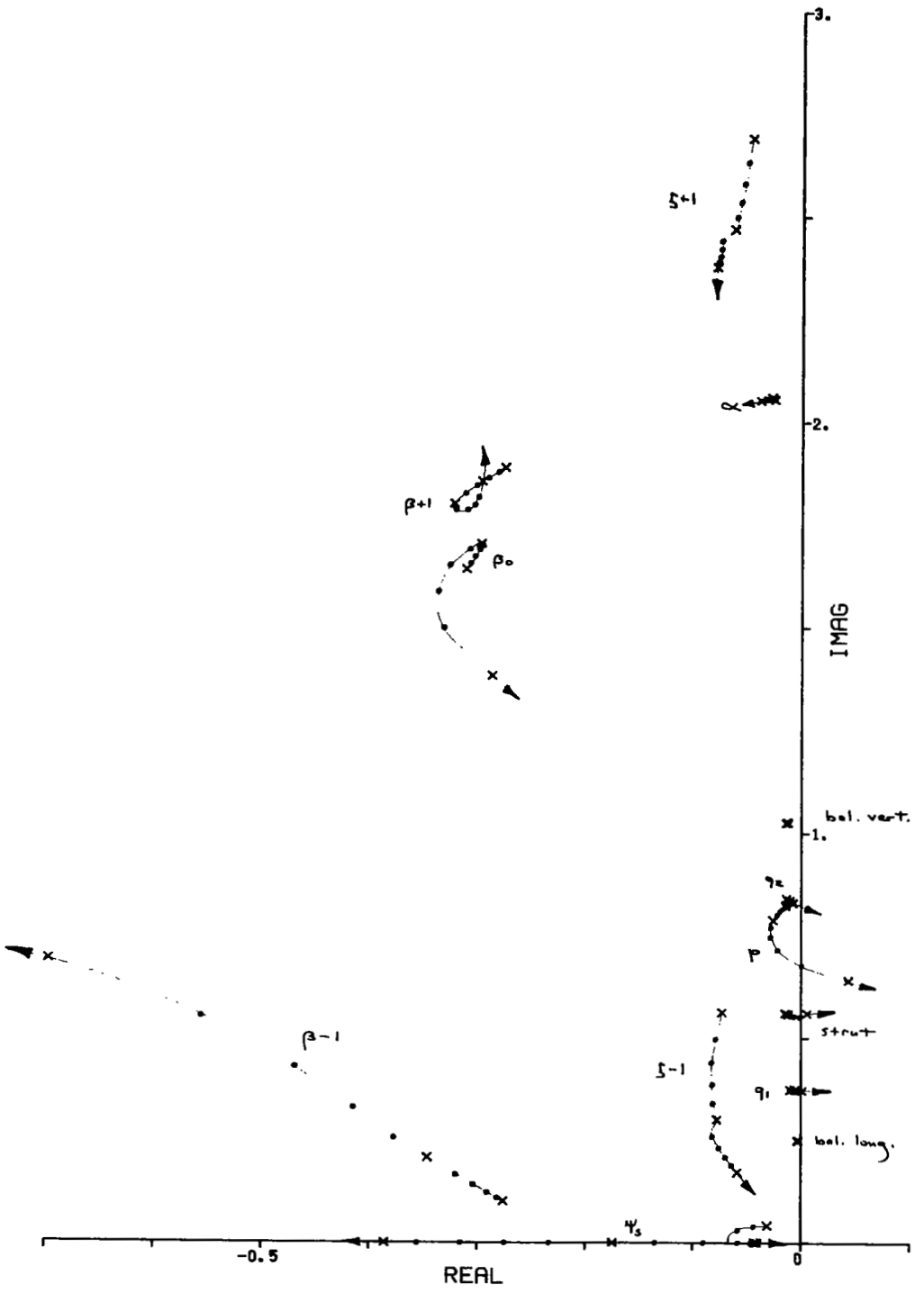

(a) Symmetric modes

Figure 20. XV-15 aircraft aeroelastic stability in the wind tunnel, root locus for V = 100 to 300 knots (ΔV = 20 knots). Airplane configuration, α_{ϕ} = 0.

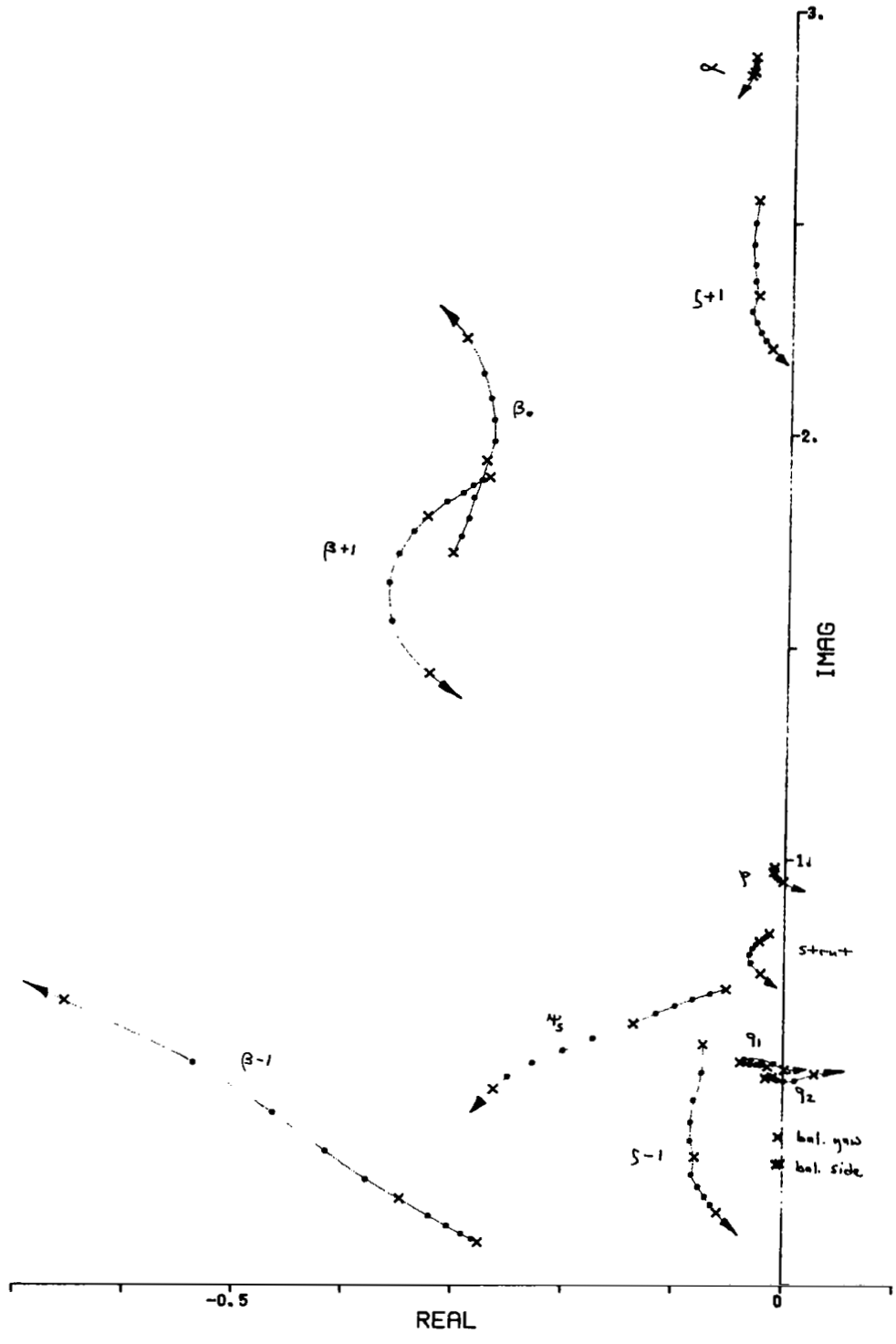

(b) Anti-symmetric modes

Figure 20. Concluded

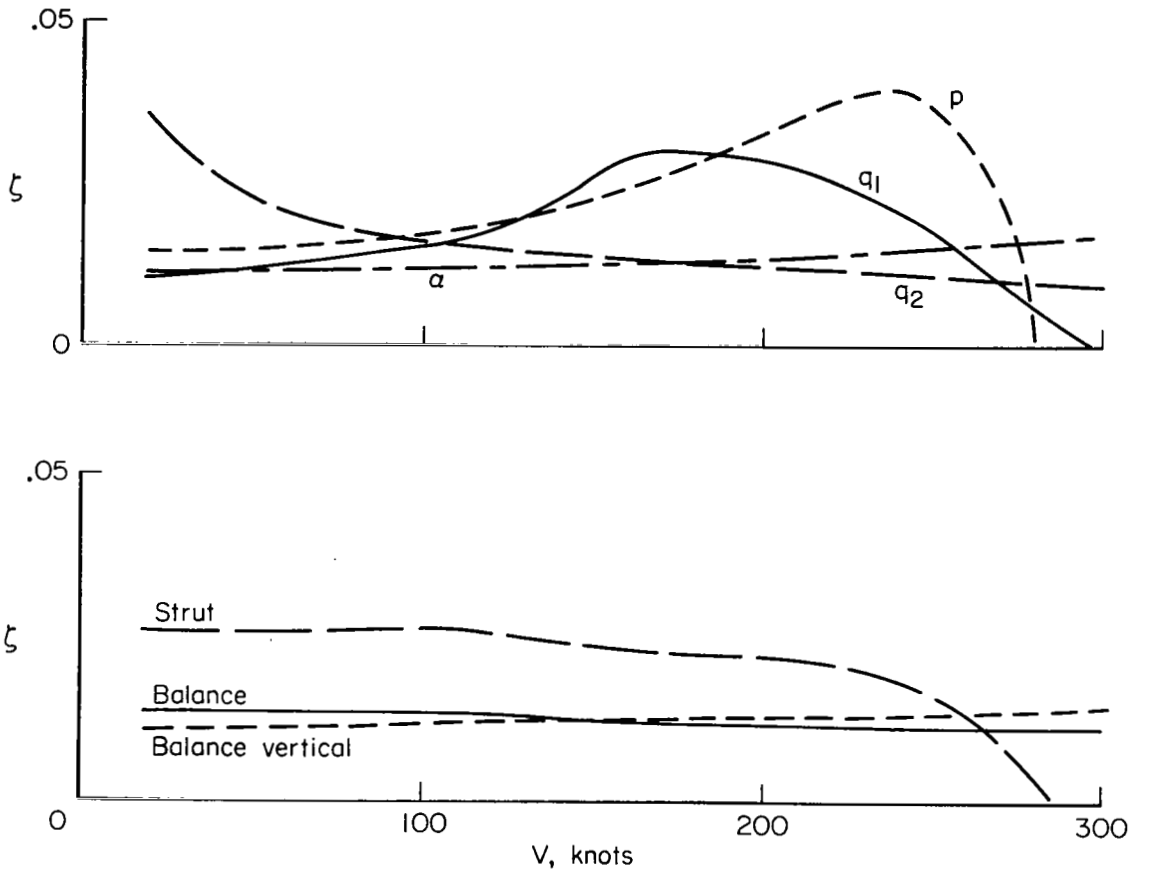

(a) Symmetric modes.

Figure 21. XV-15 aircraft aeroelastic stability in the wind tunnel: damping ratio for $\alpha_p = 0$ (airplane mode).

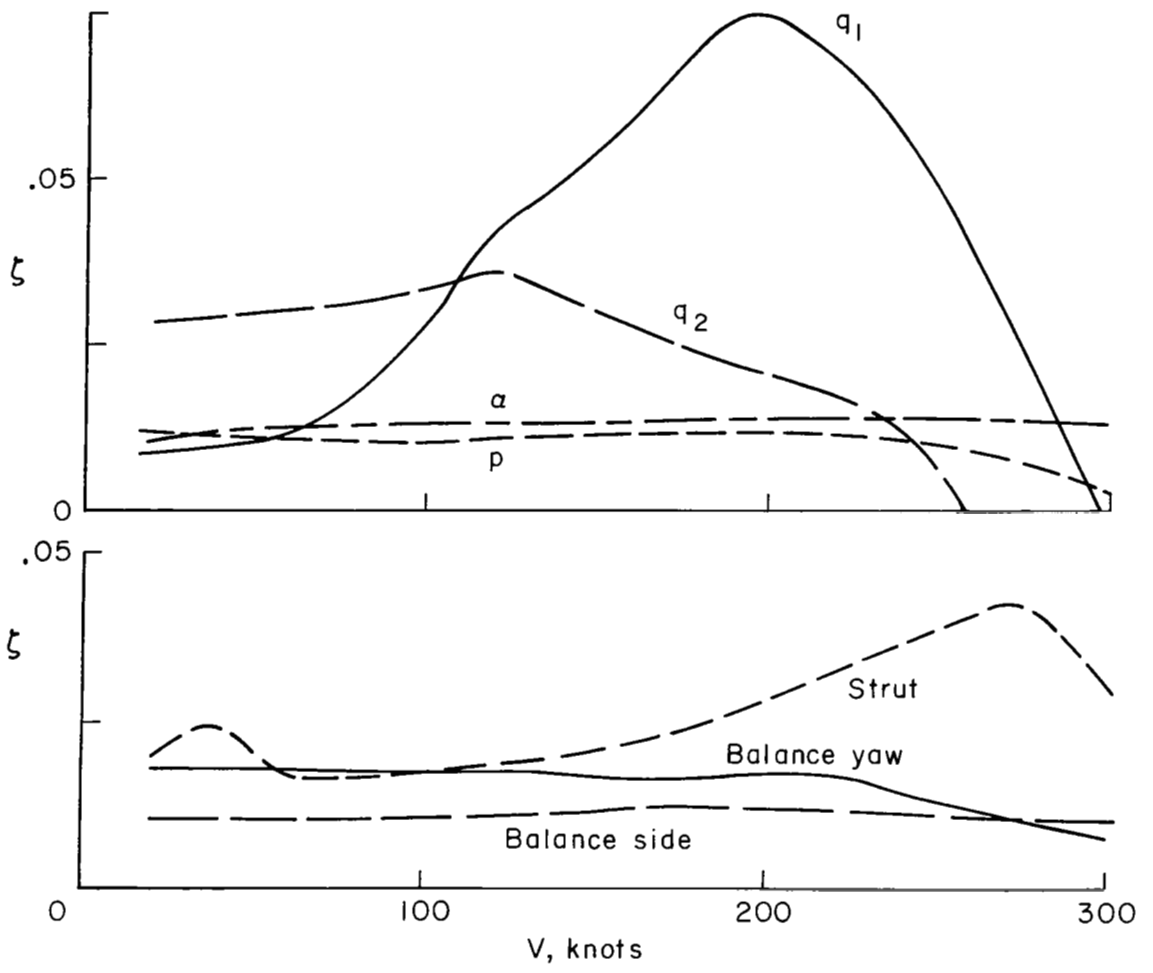

(b) Anti-symmetric modes.

Figure 21. Concluded

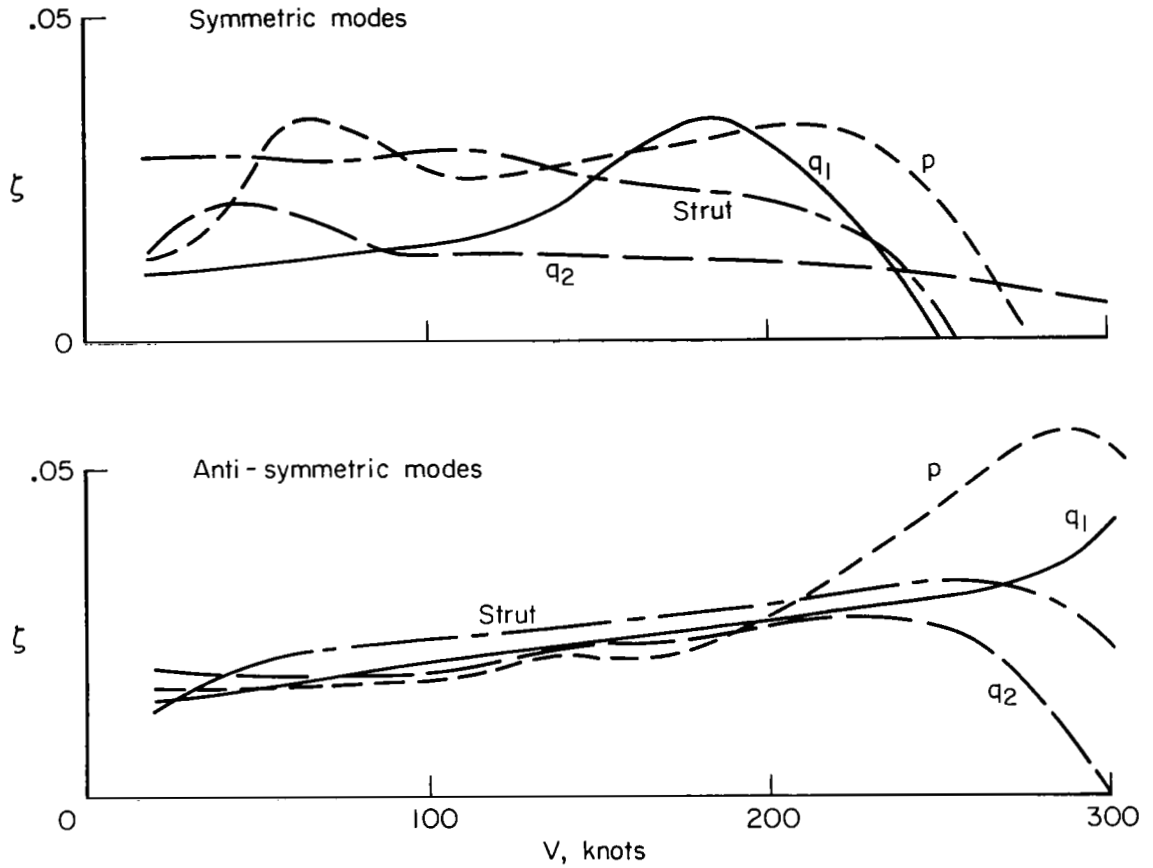

Figure 22. XV-15 aircraft aeroelastic stability in the wind tunnel: damping ratio for $\alpha_p = 0.1^\circ$ (pylon unlocked).

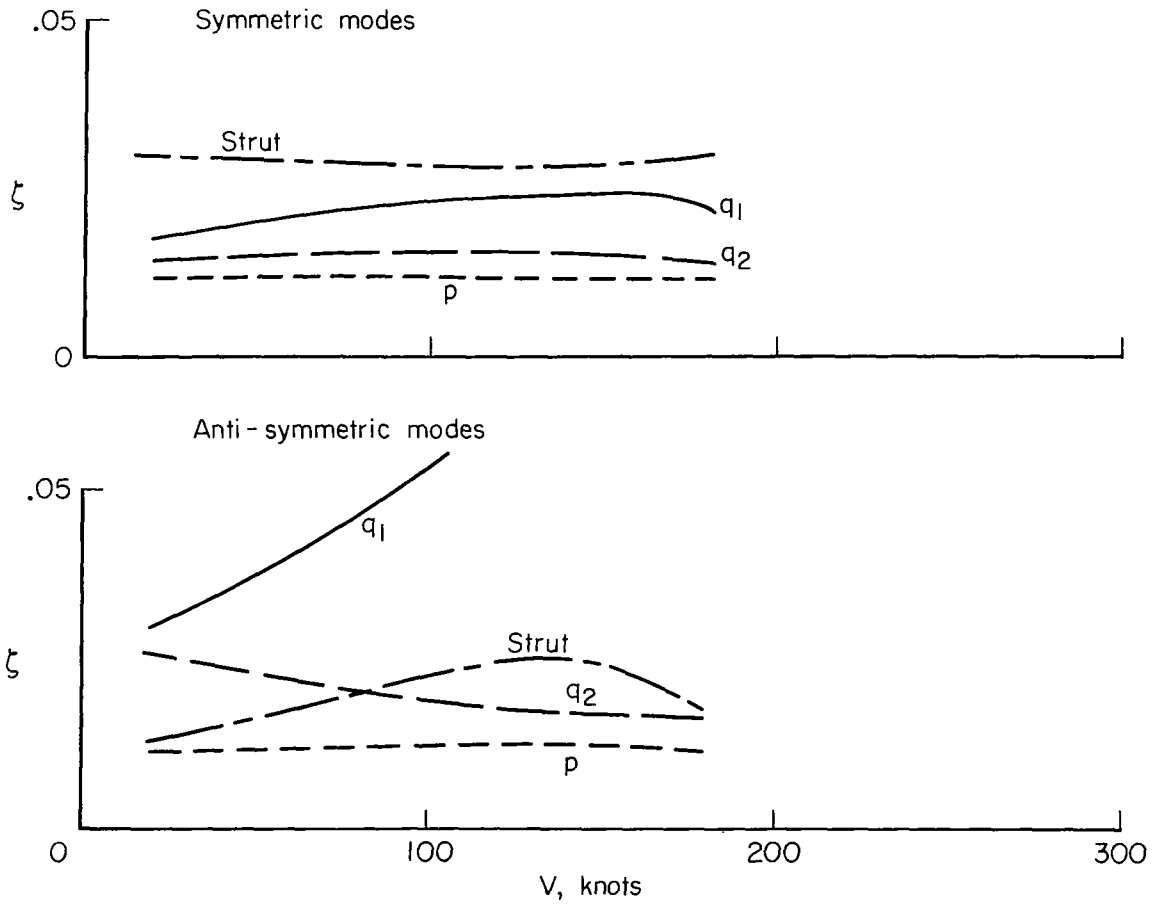

Figure 23. XV-15 aircraft aeroelastic stability in the wind tunnel: damping ratio for $\alpha_p = 30^\circ$.

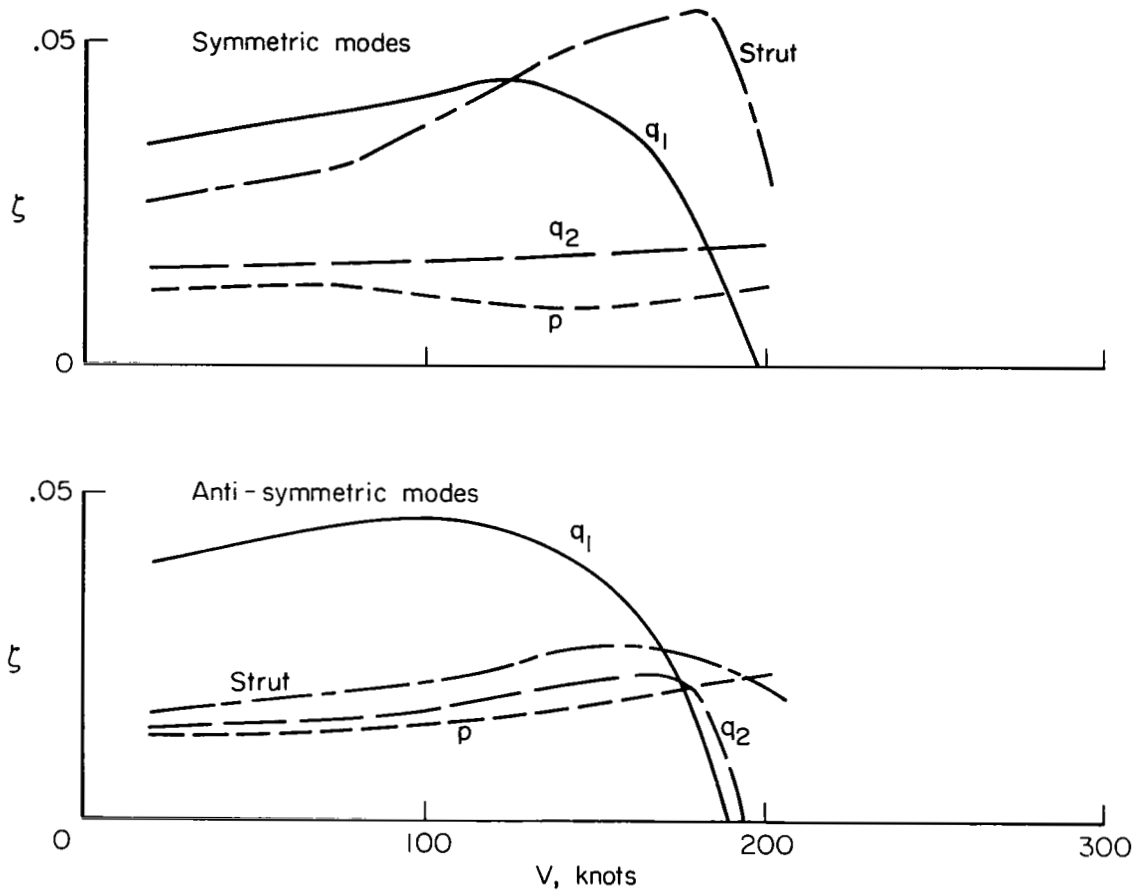

Figure 24. XV-15 aircraft aeroelastic stability in the wind tunnel: damping ratio for $\alpha_p = 60^\circ$.

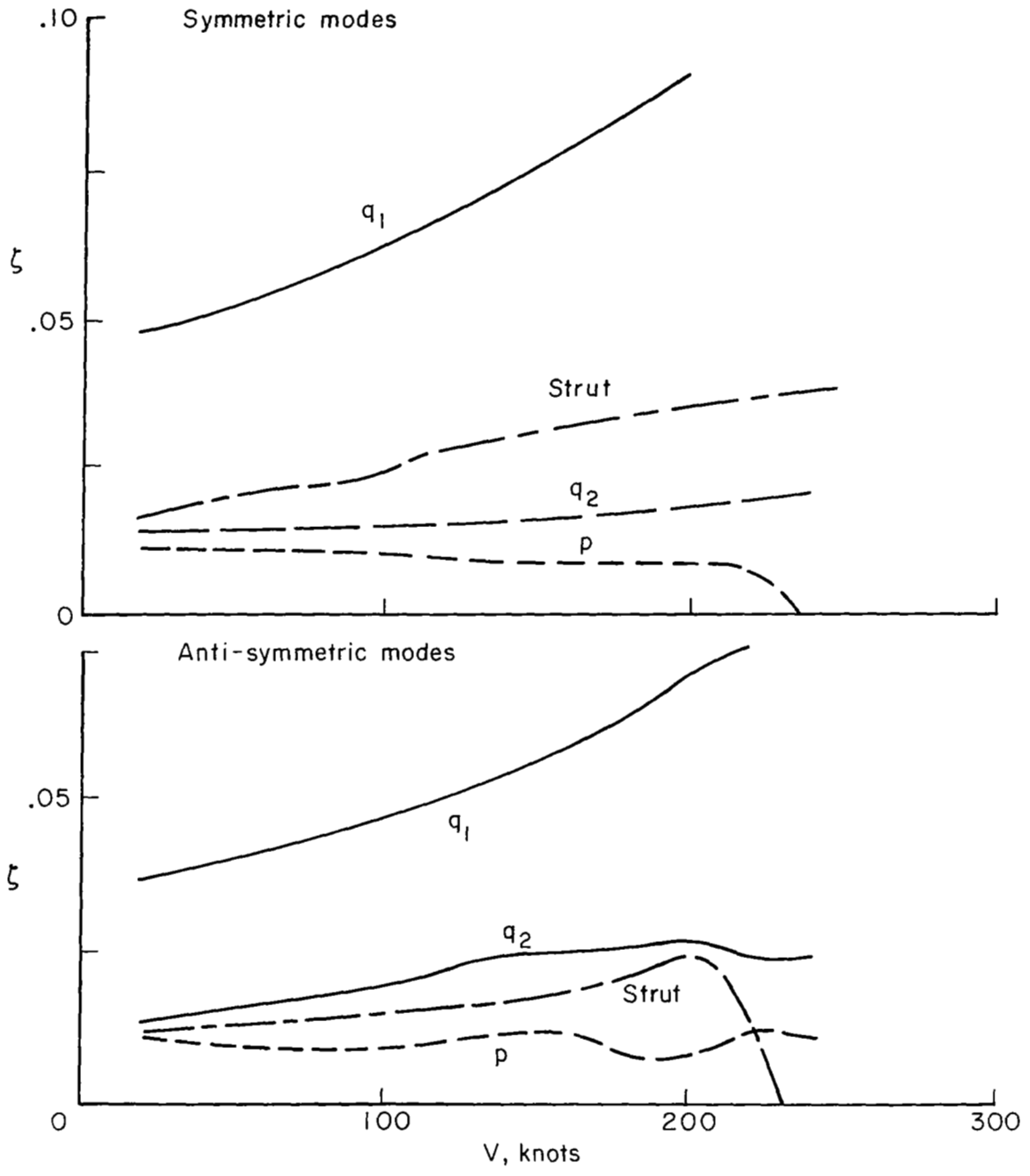

Figure 25. XV-15 aircraft aeroelastic stability in the wind tunnel: damping ratio for $\alpha_p = 90^\circ$ (helicopter mode).

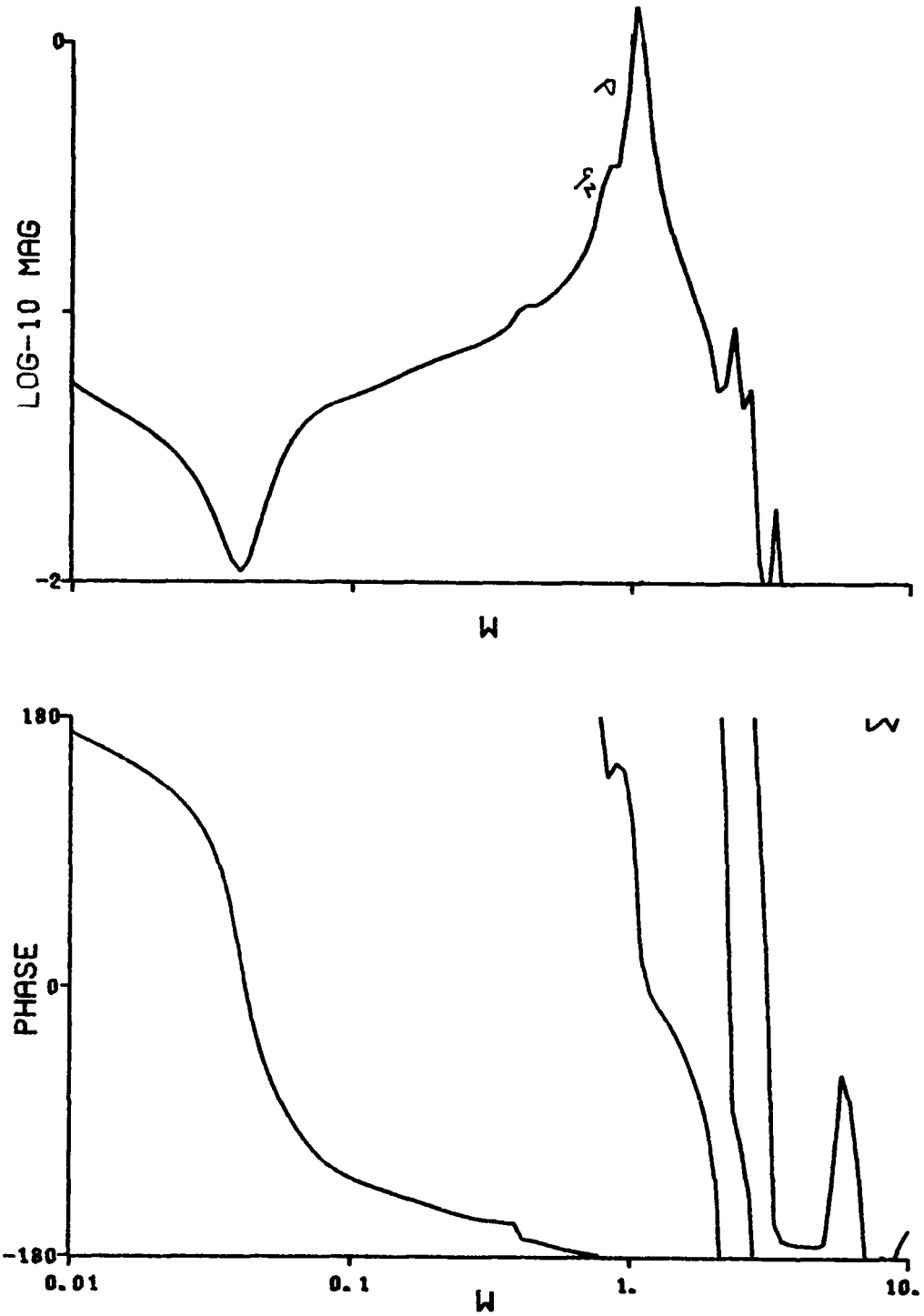

(a) Symmetric chord bending response to collective input.

Figure 26. XV-15 aircraft in flight, transfer functions of wing bending response to control (sea level cruise at V = 180 knots, $\alpha_p = 0$).

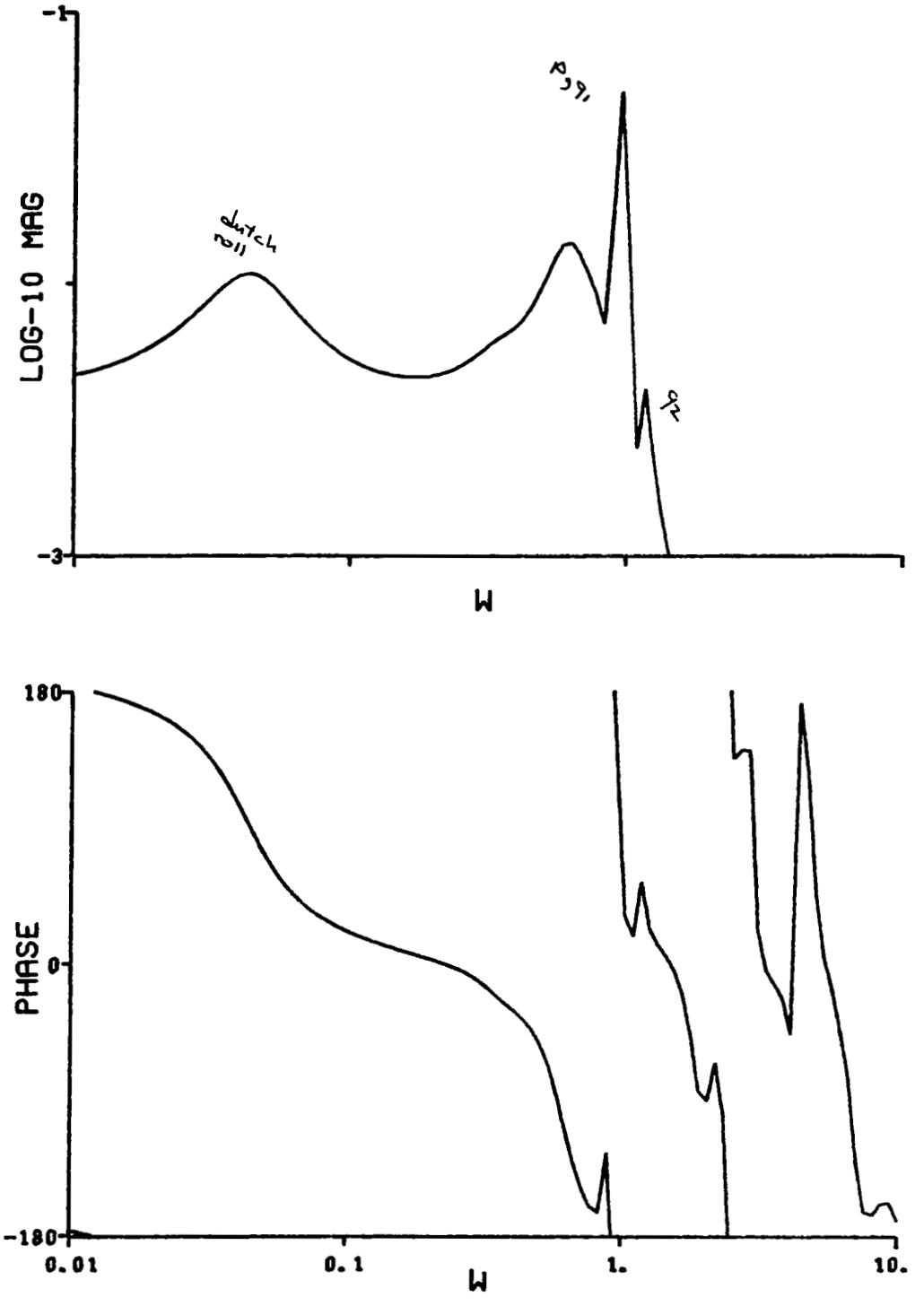

(b) Anti-symmetric chord bending response to collective input.

Figure 26. Continued

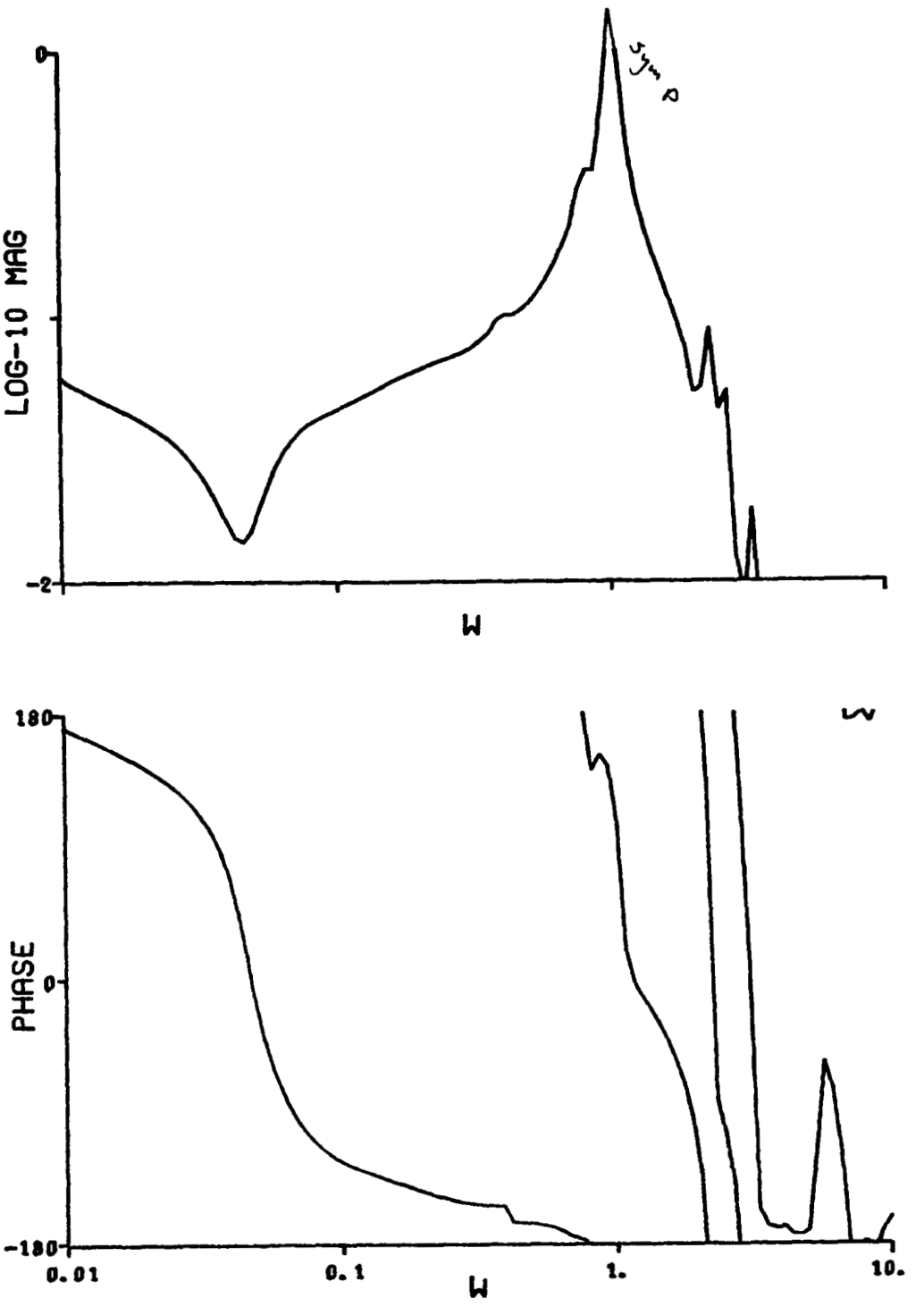

(c) Right wing chord bending response to right rotor collective input.

Figure 26. Continued

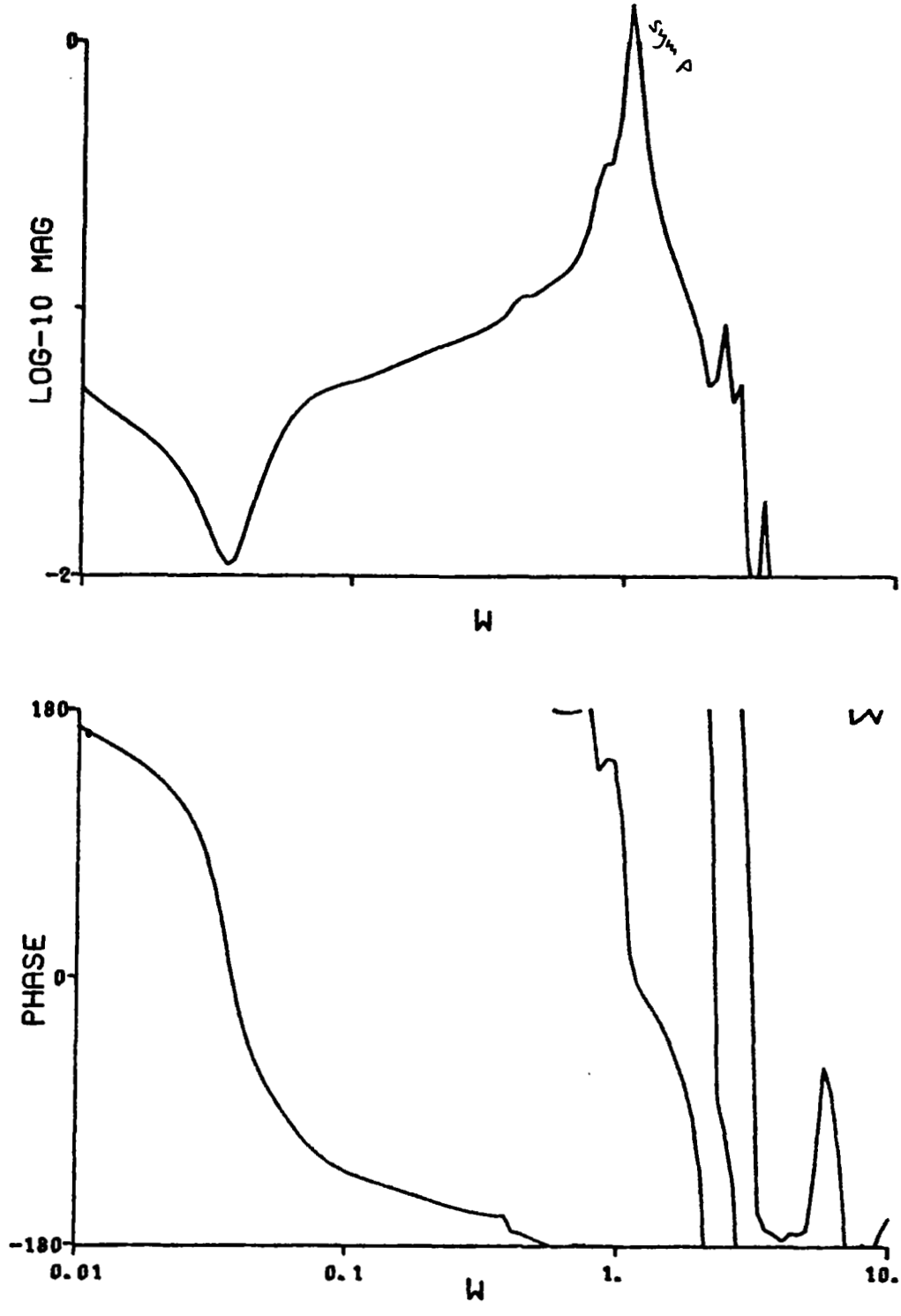

(d) Left wing chord bending response to right rotor collective input.

Figure 26. Continued

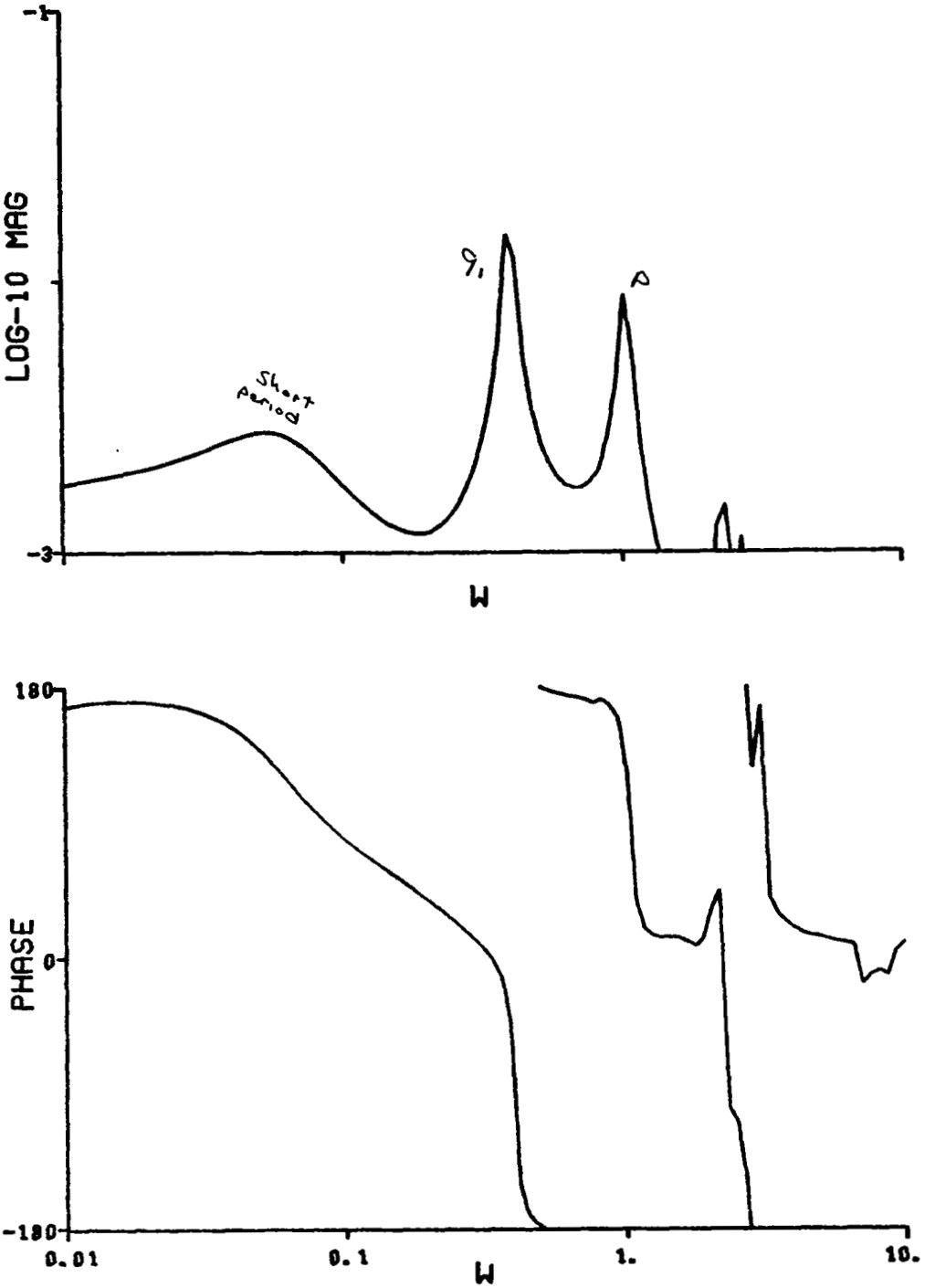

(e) Symmetric vertical bending response to flaperon input.

Figure 26. Continued

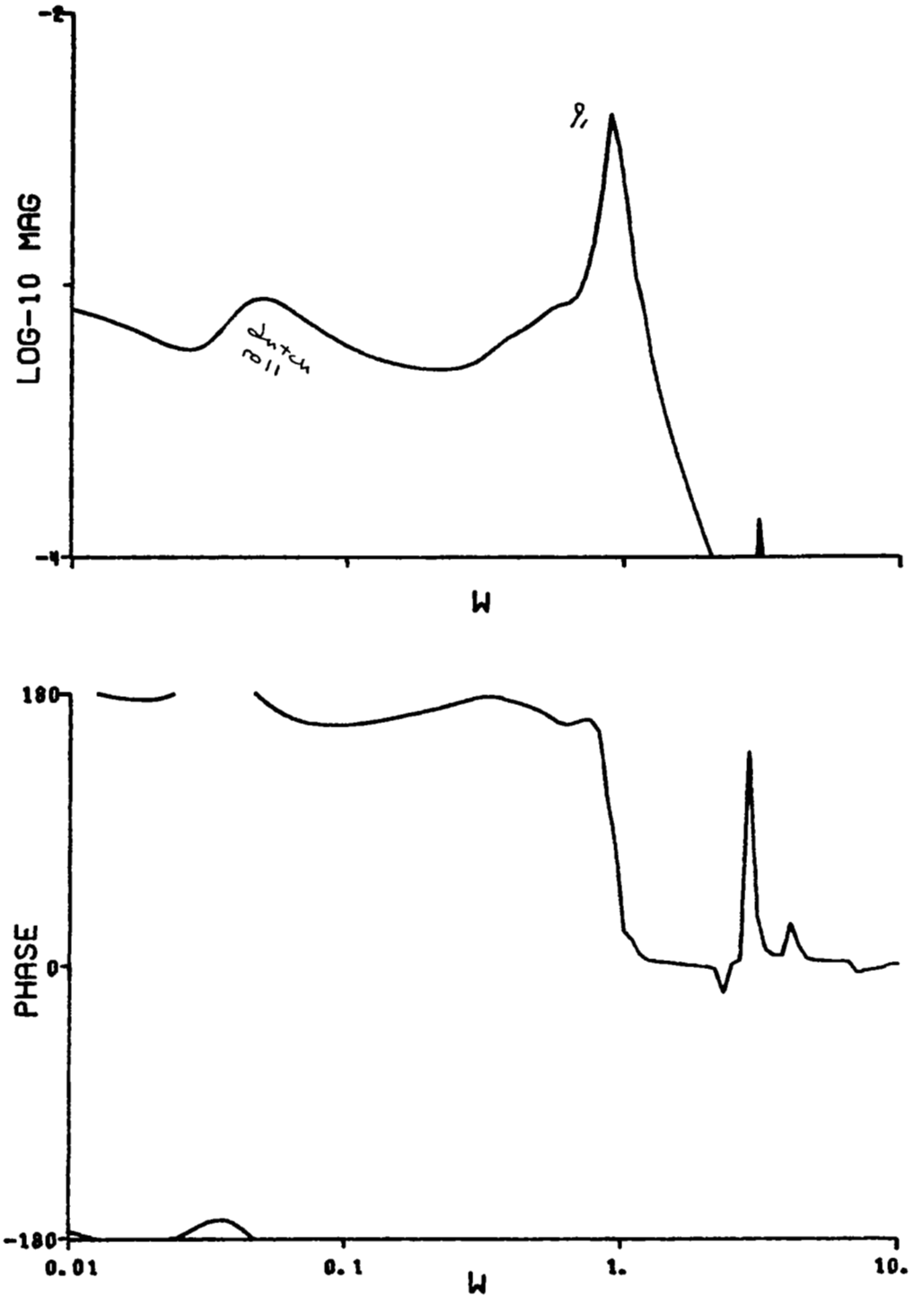

(f) Anti-symmetric vertical bending response to flaperon input.

Figure 26. Continued

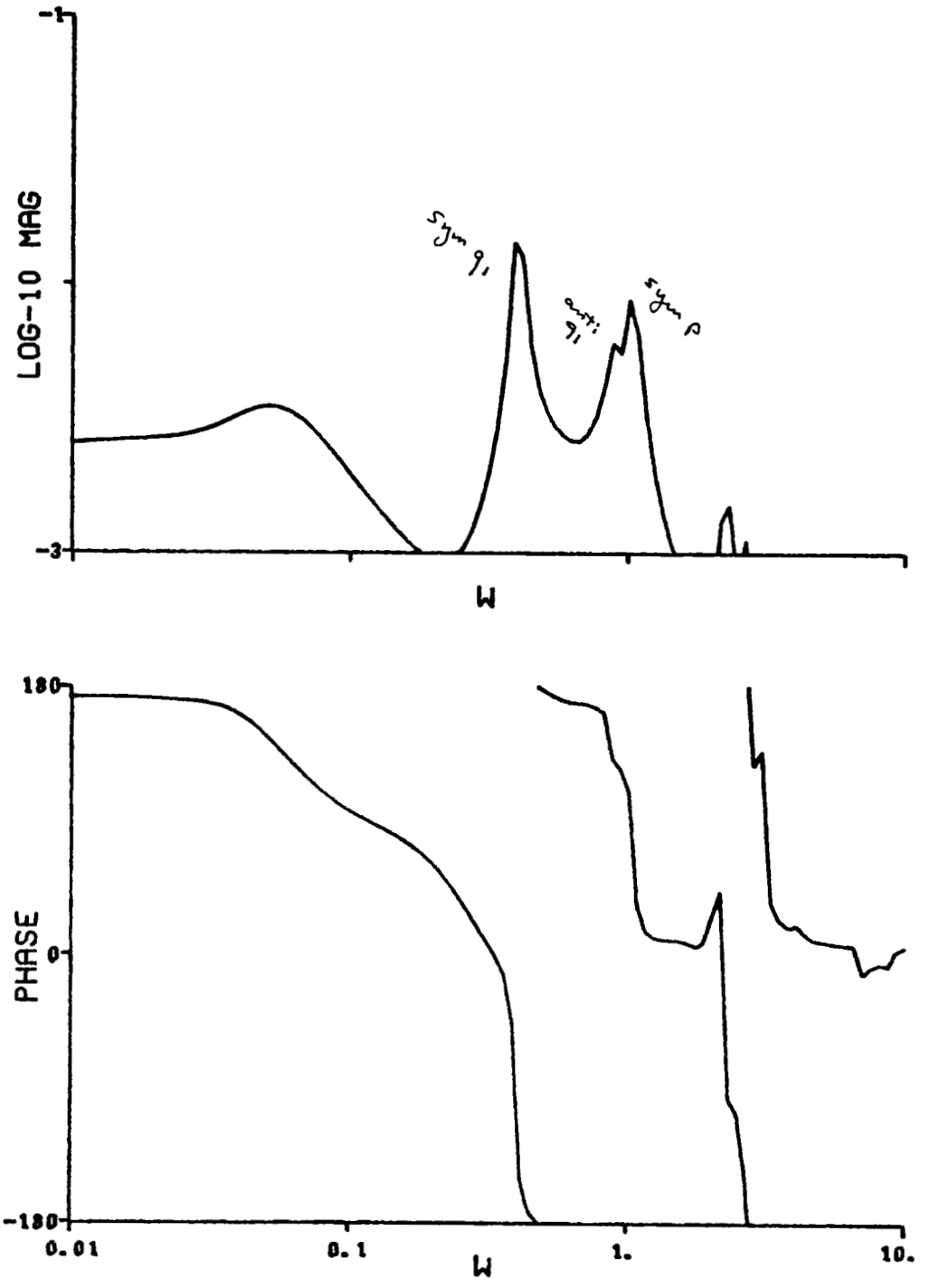

(g) Right wing vertical bending response to right wing flaperon input.

Figure 26. Continued

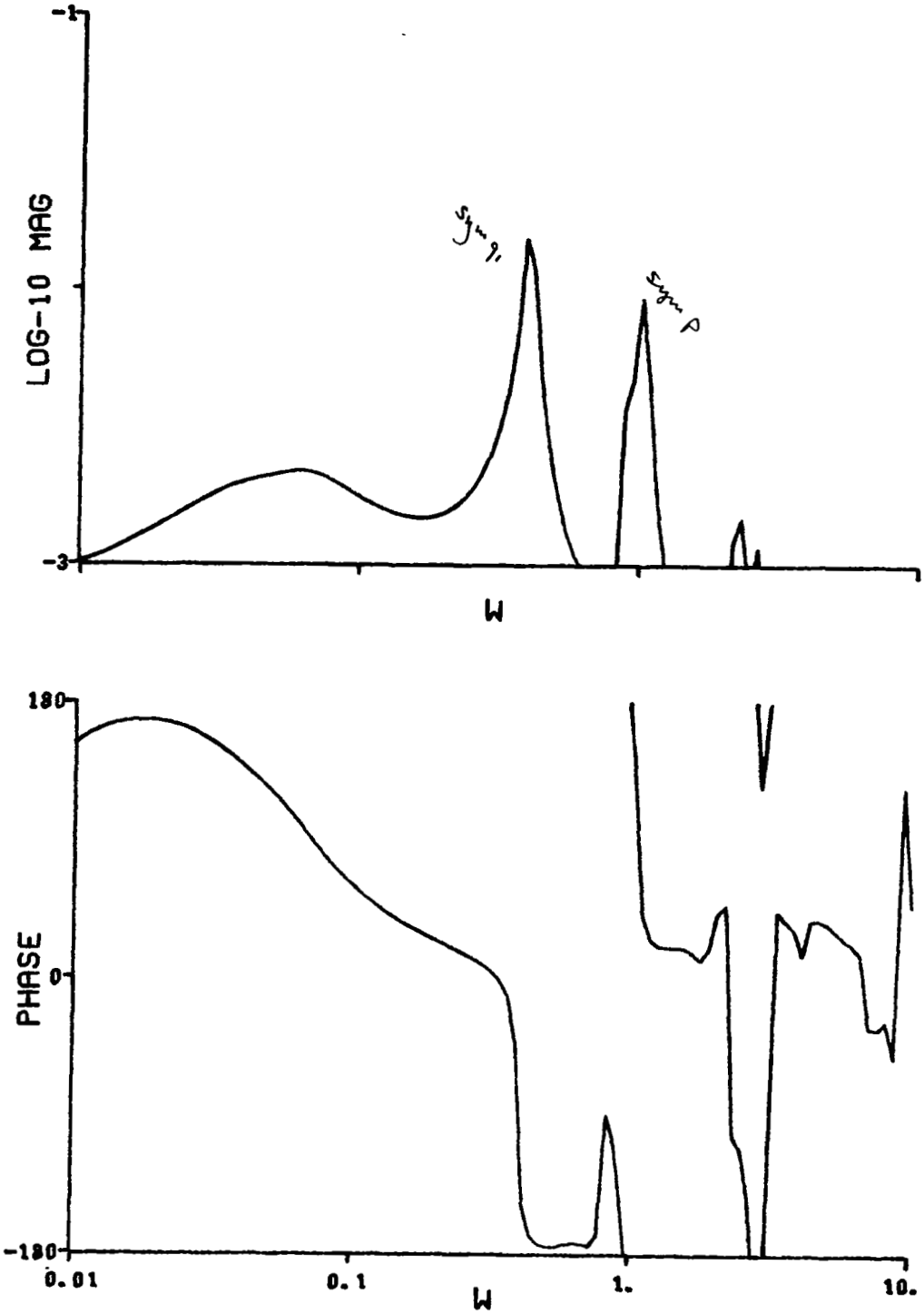

(h) Left wing vertical bending response to right wing flaperon input.

Figure 26. Concluded

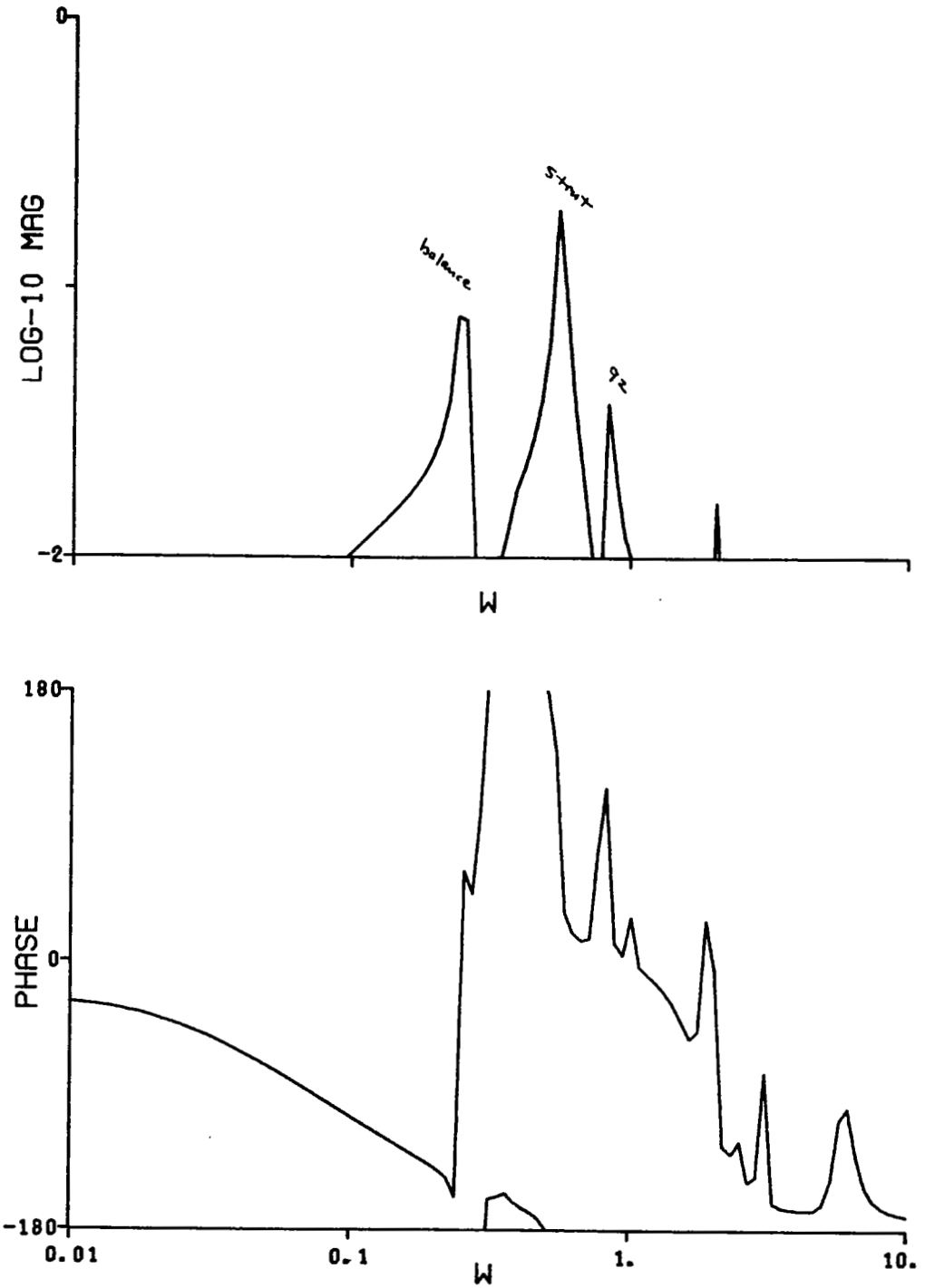

(a) Symmetric chord displacement response to collective input.

Figure 27. XV-15 aircraft in the wind tunnel, transfer functions of wing tip displacement response to control (airplane configuration at V = 180 knots, $\alpha_p = 0$).

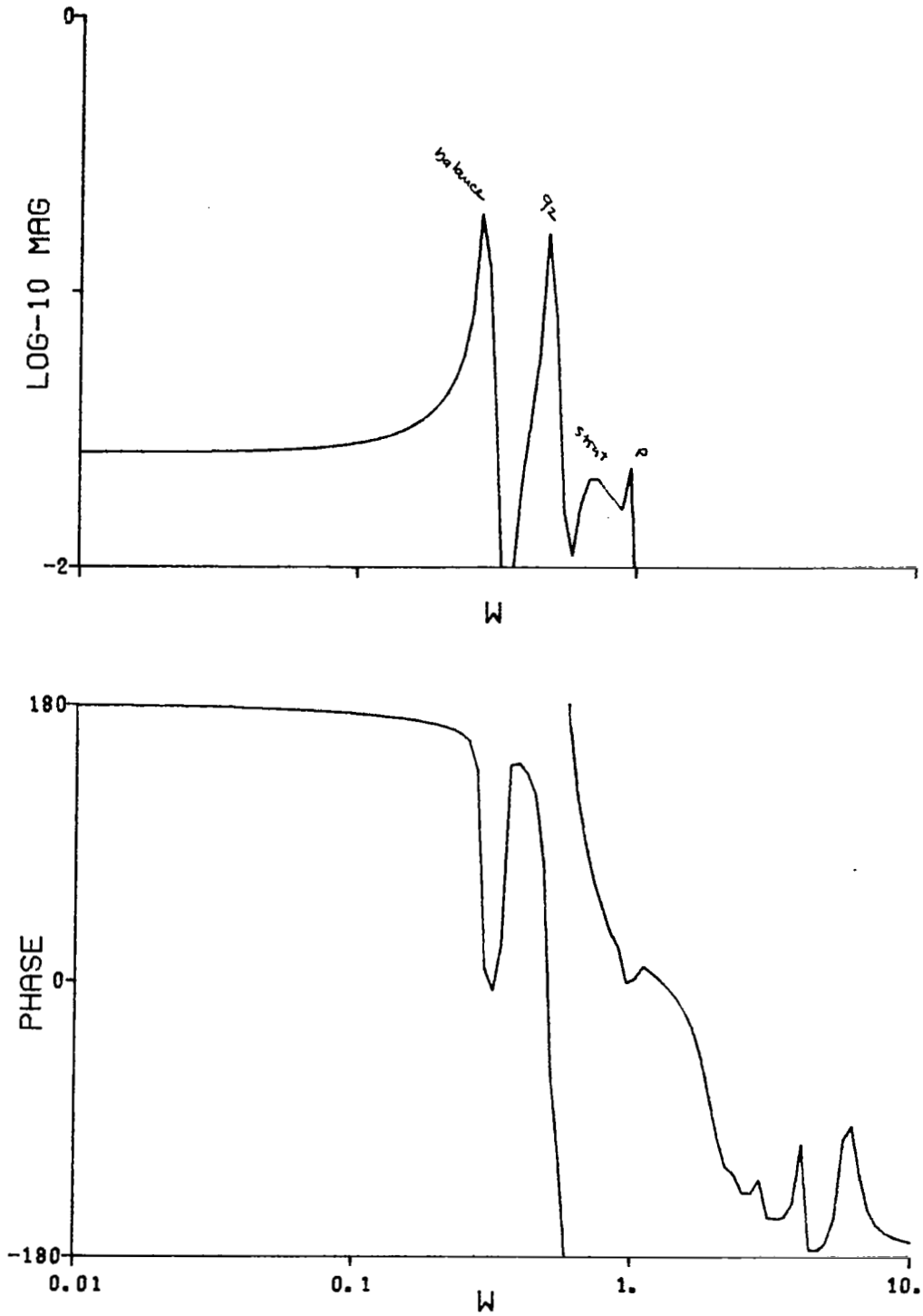

(b) Anti-symmetric chord displacement response to collective input.

Figure 27. Continued

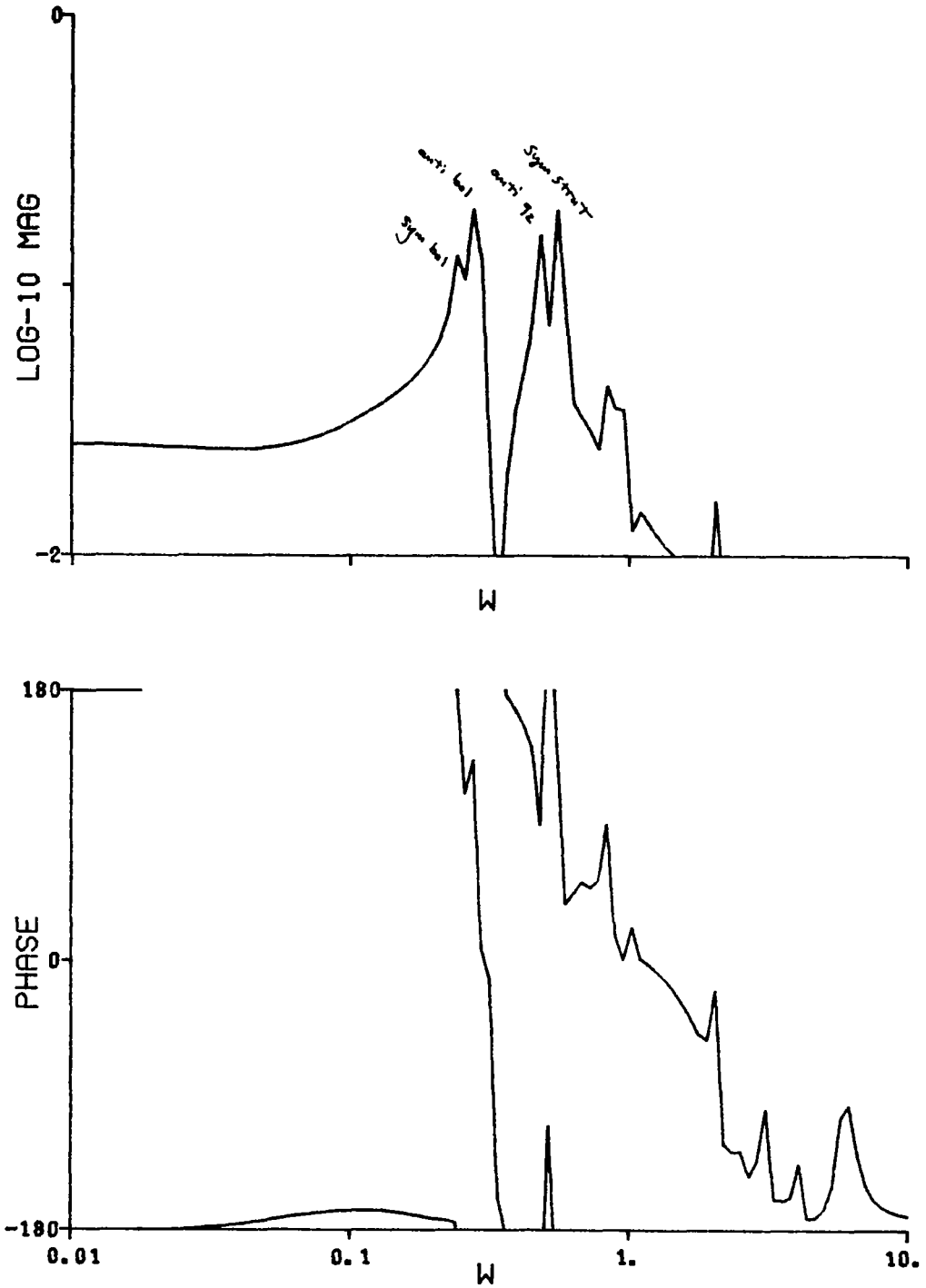

(c) Right wing chord displacement response to right rotor collective input.

Figure 27. Continued

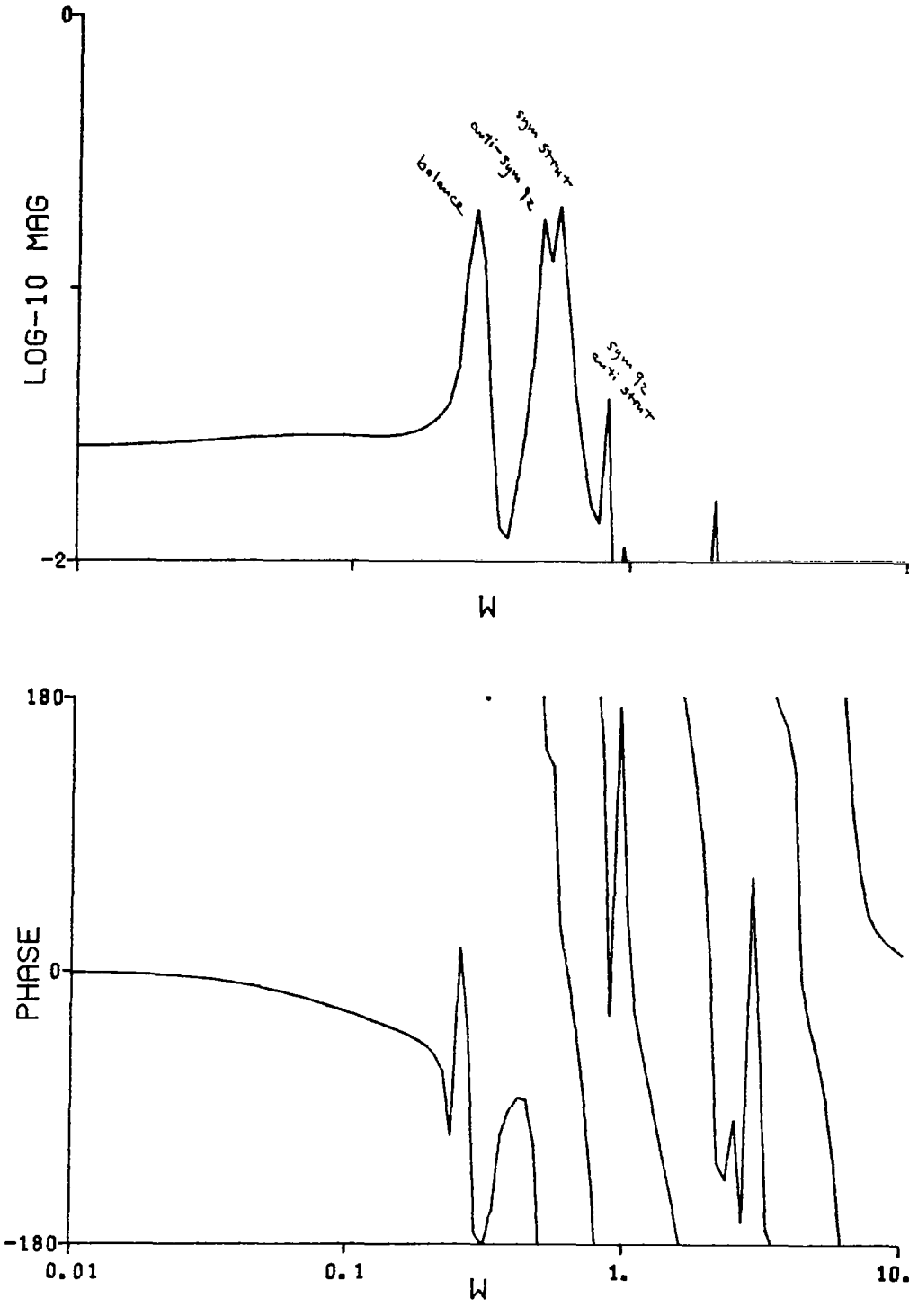

(d) Left wing chord displacement response to right rotor collective input.

Figure 27. Continued

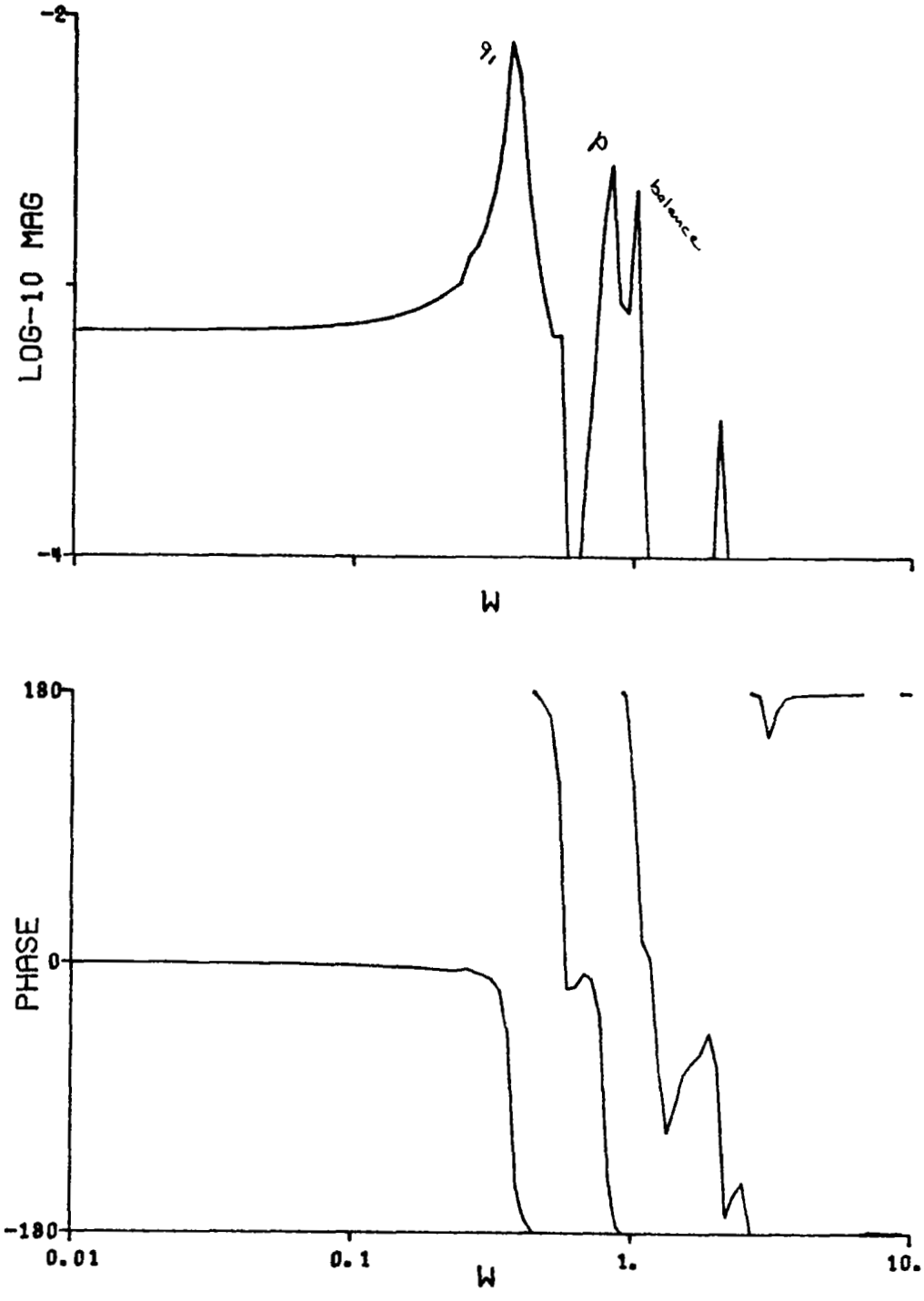

(e) Symmetric vertical displacement response to flaperon input.

Figure 27. Continued

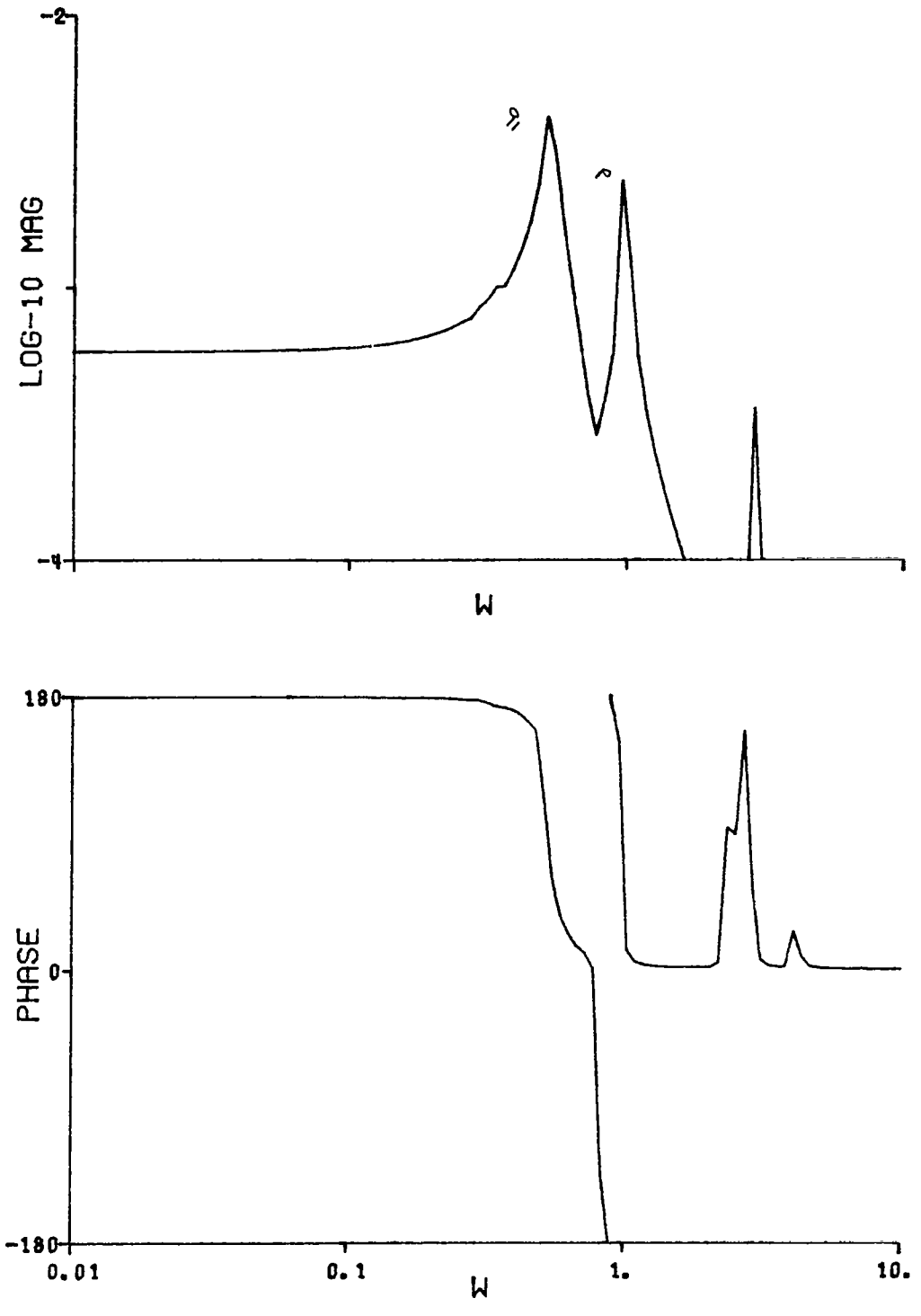

(f) Anti-symmetric vertical displacement response to flaperon input.

Figure 27. Continued

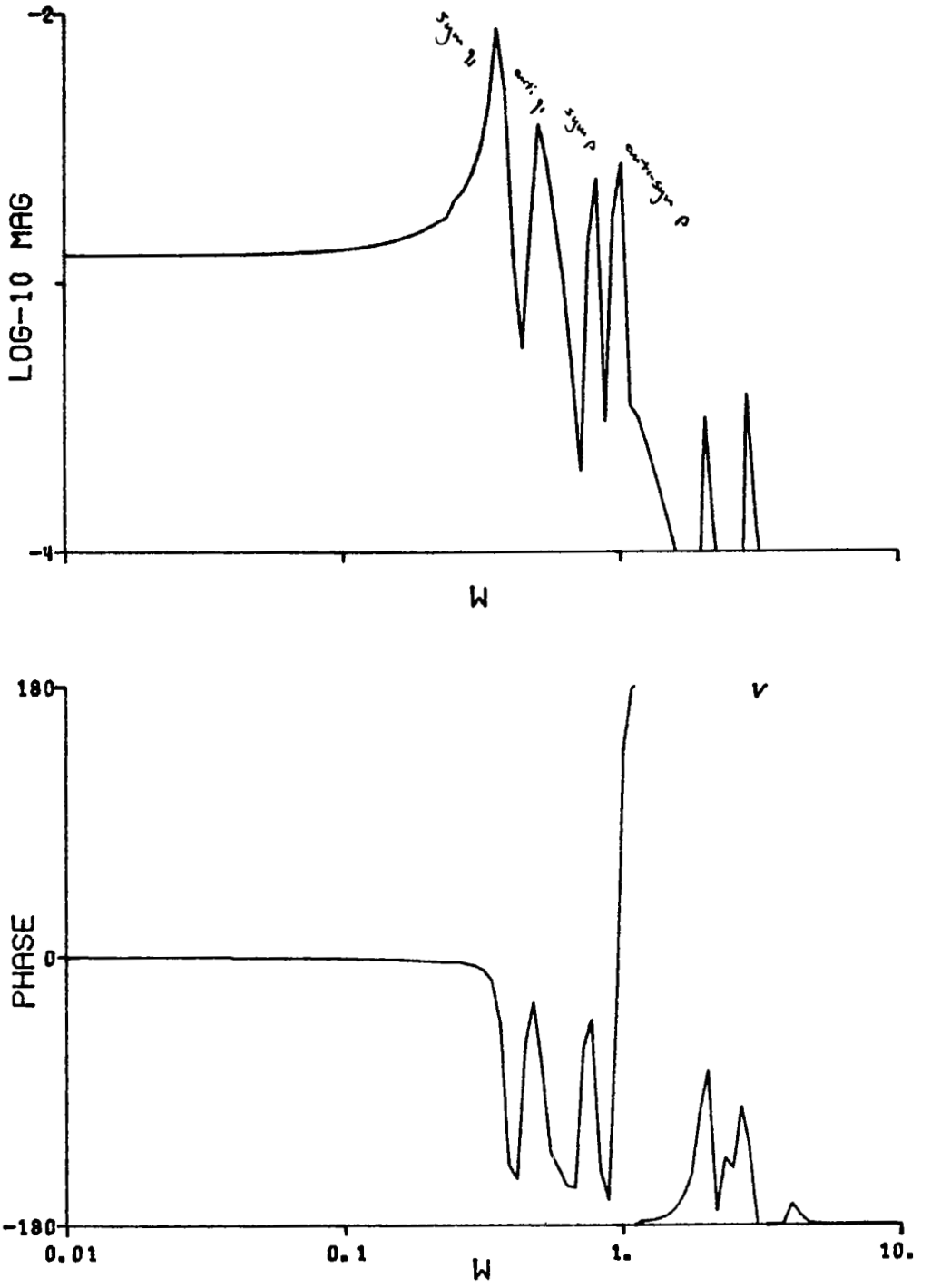

(g) Right wing vertical displacement response to right wing flaperon input.

Figure 27. Continued.

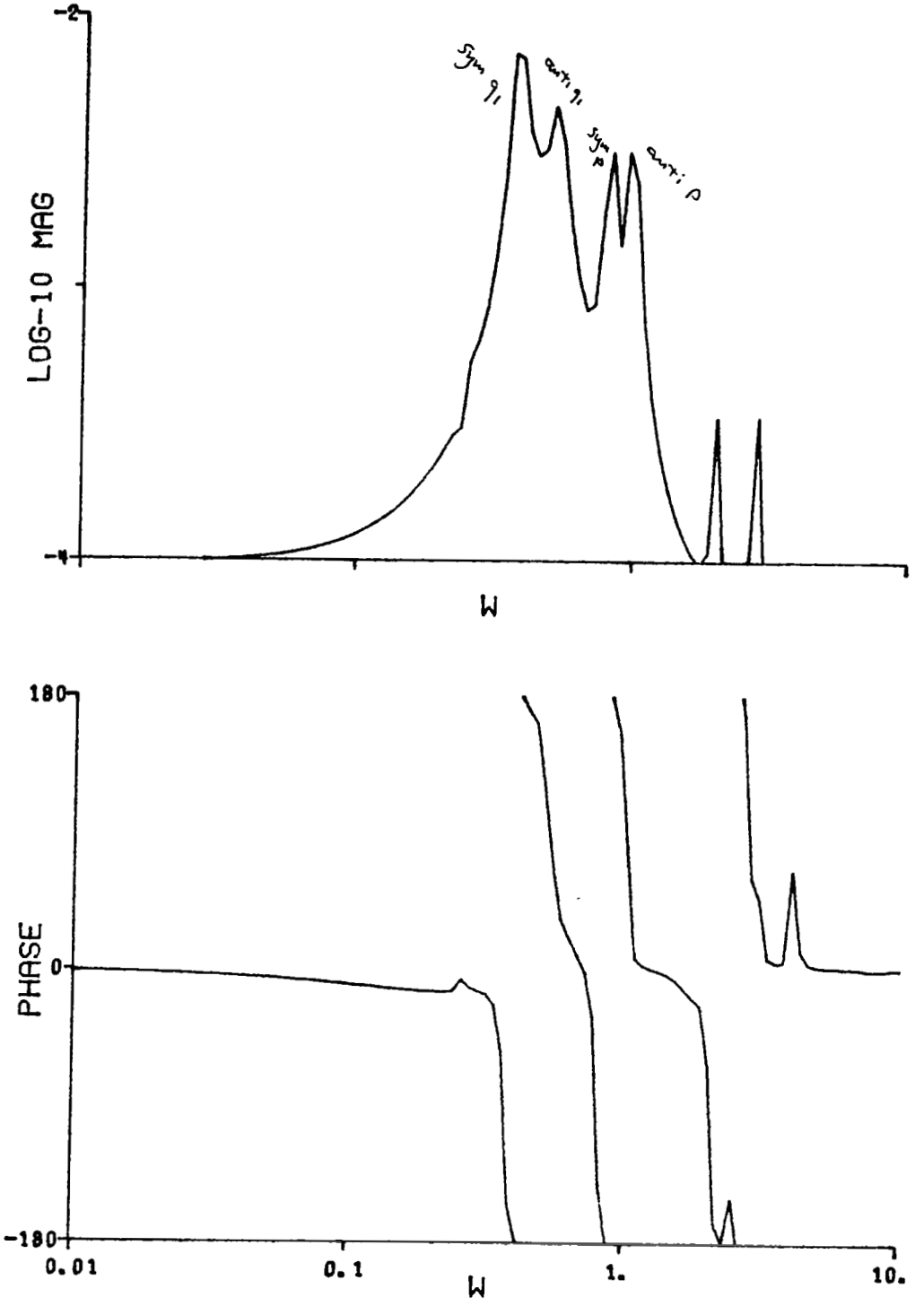

(h) Left wing vertical displacement response to right wing flaperon input

Figure 27. Concluded